A Discontinuous Galerkin Method for Diffusion Flames

Embedded in a low-Mach solver framework

Zur Erlangung des akademischen Grades Doktor-Ingenieur (Dr.-Ing.)
Vorgelegte Dissertation von Juan Francisco Gutiérrez Jorquera aus Santiago, Chile
Tag der Einreichung: 20. September 2022, Tag der Prüfung: 20. September 2022

Erstreferent: Prof. Dr.-Ing Martin Oberlack
Koreferent: Gutachter 2
Darmstadt

TECHNISCHE
UNIVERSITÄT
DARMSTADT

Fachbereich Maschinenbau
Fachgebiet für
Strömungsdynamik

A Discontinuous Galerkin Method for Diffusion Flames
Embedded in a low-Mach solver framework

Vorgelegte Dissertation von Juan Francisco Gutiérrez Jorquera

Erstreferent: Prof. Dr.-Ing Martin Oberlack
Koreferent: Gutachter 2

Tag der Einreichung: 20. September 2022
Tag der Prüfung: 20. September 2022

Darmstadt

Bitte zitieren Sie dieses Dokument als:
URN: urn:nbn:de:tuda-tuprints-1234
URL: http://tuprints.ulb.tu-darmstadt.de/12345
DOI: https://doi.org/10.25534/tuprints-1234

Dieses Dokument wird bereitgestellt von tuprints,
E-Publishing-Service der TU Darmstadt
http://tuprints.ulb.tu-darmstadt.de
tuprints@ulb.tu-darmstadt.de

Dedication

Erklärungen laut Promotionsordnung

§8 Abs. 1 lit. c PromO

Ich versichere hiermit, dass die elektronische Version meiner Dissertation mit der schriftlichen Version übereinstimmt.

§8 Abs. 1 lit. d PromO

Ich versichere hiermit, dass zu einem vorherigen Zeitpunkt noch keine Promotion versucht wurde. In diesem Fall sind nähere Angaben über Zeitpunkt, Hochschule, Dissertationsthema und Ergebnis dieses Versuchs mitzuteilen.

§9 Abs. 1 PromO

Ich versichere hiermit, dass die vorliegende Dissertation selbstständig und nur unter Verwendung der angegebenen Quellen verfasst wurde.

§9 Abs. 2 PromO

Die Arbeit hat bisher noch nicht zu Prüfungszwecken gedient.

Darmstadt, 20. September 2022

J. Gutiérrez-Jorquera

Abstract

Abstract

Zusammenfassung

Zusammenfassung

Acknowledgements

Acknowledgements

Contents

List of Figures

List of Tables

List of Abbreviations

$\mathbf{u}_{\mathbf{ext}}$	Extension-velocity field

List of Symbols

Ω	Domain of interest, computational domain
$\partial\Omega$	Domain boundary
$\mathfrak{A}$	Bulk phase A
$\mathfrak{B}$	Bulk phase B
$\mathfrak{s}$	Bulk phase, species
$\Omega \setminus \mathfrak{I}$	Bulk
$\mathfrak{I}$	Interface
$\mathbf{w}$	Singular surface velocity vector
w	Normal component of the singular surface velocity
$\mathbf{u}_\mathfrak{I}$	Material interface velocity vector
$\mathbf{n}_{\partial\Omega}$	Outer boundary normal vector
$\mathbf{n}_\mathfrak{I}$	Interface normal vector
$\mathbf{n}$	Normal vector
$\boldsymbol{\tau}$	Tangent vector
$\mathbf{P}_\mathfrak{I}$	Interface projection tensor
$\mathbf{P}$	Projection tensor
$\mathbf{u}$	Velocity vector
p	Pressure
$e_{\mathbf{kin}}$	Kinetic energy
e_σ	Surface energy
ψ	General field/physical property
$\mathbf{f}$	Flux vector
μ	Dynamic viscosity
ν	Kinematic viscosity
σ	Surface tension coefficient
κ	Mean curvature
$\mathbf{D}$	Rate of deformation tensor
$\mathbf{S}$	Stress tensor
θ	Apparent contact angle
$\theta_{\mathbf{stat}}$	Static contact angle
L	Contact line
$l_{\mathbf{cap}}$	Capillary length
$l_{\mathbf{s}}$	Slip length
$\mathbf{n}_L$	Contact line normal vector
U_L	Contact line velocity
β	Coefficient of friction
c_p	Specific heat capacity of the mixture

$c_{p,k}$	Specific heat capacity of species k
T	Temperature
$T_{\mathbf{sat}}$	Saturation temperature
$\mathbf{q}$	Heat flux vector
c	Specific heat capacity
k	Thermal conductivity
ρ	Density
$\dot{m}$	Mass transfer rate
$h_{\mathbf{vap}}$	Enthalpy/(latent) heat of vaporization
D	Diffusion coefficient
ν_k	Stoichiometric coefficient of species k
A	Aggregation map
Agg	Aggregation mesh
N_k	Number of local DOF
N	Number of total DOF
$\mathbf{Op}$	Operator matrix
k	Total degree of the polynomial space
α	Aggregation threshold
ϕ	Basis function
$\mathbb{P}_k$	Broken polynomial space
K	Numerical cell
$K^{\mathbf{X}}$	Numerical cut-cell
$\mathbf{X}$	Cut
Δt	Time step size
$\Gamma_{\mathbf{D}}$	Edge imposed with Dirichlet boundary condition
$\Gamma_{\mathbf{int}}$	Internal edge
$\Gamma_{\mathbf{N}}$	Edge imposed with Neumann boundary condition
Γ	Edge
h	Numerical mesh size
$\mathfrak{K}_{\mathbf{cc}}$	Set of cut-cells
$\mathfrak{K}_{\mathbf{far}}$	Set of far-field cells
$\mathfrak{K}_{\mathbf{near}}$	Set of cut-cell neighbours
$\mathfrak{K}_h^{\mathbf{X}}$	Numerical cut-cell mesh
$\mathfrak{K}_h$	Numerical mesh
φ	Level-set function
Edg	Logical edge
$\mathbf{M}$	Mass matrix
$\mathbf{n}_\Gamma$	Edge normal field
$\mathbf{n}_{\mathfrak{I},\Gamma}$	Edge normal field including the interface normal vector
$\hat{F}$	Numerical flux
$\varphi^{\mathbf{dg}}$	Level-set function represented by a DG field
$\varphi^{\mathbf{c0}}$	Constrained level-set function represented by a DG field
η	Penalty parameter
$\mathbb{V}_{\mathbf{k}}^{\mathbf{X}}$	Sum of broken polynomial spaces
ϑ	General test function

q	Test function for the continuity equation
r	Test function for the heat equation
$\mathbf{v}$	Test function for the momentum equation
ER	Expansion ratio the backward-facing step
Eo	Eötvös number
La	Laplace number
Pe	Peclet number
Fr	Froude number
ω	Oscillation frequency
λ	Wavelength
k	Wavenumber
g	Gravity vector
h	Channel heigth of the backward-facing step
λ	Heat conductivity
h_k	Specific enthalpy of k species.
Y_k	Mass fraction of species k
W	Mean molecular weight of the mixture
W_k	Molecular weight of species k
N	Total number of species in the mixture
Nu	Nusselt number, local
ω_k	Net rate of production of species k
Pr	Pradntl number
p	Pressure
$\mathcal{R}$	Universal gas constant
Re	Reynolds number
S	Step heigth of the backward-facing step
τ	Viscous tensor
t	Time
u	Velocity vector
D	Diffusion coefficient
U	Diffusion velocity vector

1 Introduction

hmm

1.1 Introduction and state of the art.

1.1.1 Combustion

Premixed Flames(???)

Non-Premixed Flames

Droplet(?)

High order discretization methods is a topic which has been gaining increasing attention in the last decades. An important exponent of them is the Discontinuous Galerkin (DG) method Cockburn et al., 2000. The DG method was initially developed and utilized for solving hyperbolic conservation laws, especially in the field of computational fluid dynamics (CFD), and has recently gained increased attention for incompressible CFD problems for structured and unstructured grids. Two main advantages stand out when compared with traditional methods such as the Finite Volume Method (FVM) or the Finite Difference Method (FDM): First, DG offers an arbitrary order of error convergence due to the polynomial local approximation of the solution field. A polynomial approximation of degree p provides a numerical discretization error of the order $\mathcal{O}(h^{p+1})$ for sufficiently smooth solutions, where h is a characteristic grid length. Secondly, regardless of the desired order of accuracy, any given cell of the grid only requires information from its immediate neighbours, allowing for efficient parallelization with minimal communication overhead. In contrast, more traditional schemes, such as the FVM, are usually limited to $\mathcal{O}(h^N)$ accuracy, with $N \leq 2$ for unstructured grids. Even for structured grids N is practically limited to low values due to the increasing stencil size for increasing N. Advantageously the DG method offers the locality of low-order schemes and the accuracy per degree of freedom of spectral schemes.

In the context of CFD solvers, an important distinction is that between pressure-based and density-based solvers. Historically, pressure-based solvers have been used for incompressible flows, i.e. flows with divergence-free velocity fields. On the other hand, density-based (also called fully compressible) solvers should, in theory, be able to solve flows in all Mach number ranges. However, in practice, as the Mach number approaches zero, density-based solvers experience efficiency and accuracy problems. These issues are mainly attributed to the acoustic effects in the flow, which tends to generate very stiff systems. None of these approaches are directly applicable to flows with varying density in the low-Mach limit. Hennink et al., 2021 It is possible, however, to extend existing incompressible and compressible codes so that they are capable of dealing with low Mach numbers. Keshtiban et al., 2003 In this work a extension from a incompressible solver is presented.

There are numerous works in which the DG method has been used within the context of incompressible flows. Shahbazi et al., 2007; Kummer, 2012; Klein et al., 2013; Rhebergen et al., 2013 However, there are not many publications in which the flow problem at low Mach numbers is addressed using a pressure-based solver. In the work by Klein et al. Klein et al., 2016 the low-Mach equations are solved in a DG Framework making use of a SIMPLE type scheme. The solution of a time-step involves an iterative process that requires multiple matrix assemblies and solutions. The obtained systems of equations are solved by means of fixed-point iterations, where relaxation factors are necessary to obtain convergence of the computations. In the work of Hennink et al. Hennink et al., 2021 a pressure-based solver for low-mach flows is presented. They solve the mass flux instead of the velocity as the primitive variable.

High order methods are very attractive for complex reacting fluid dynamical systems, where usually a high numerical resolution is necessary. Particularly for combustion problems, where large amounts of heat are released in rather small zones within the flow, the high number of elements required to resolve the resulting steep gradients could result in prohibitive calculation times even for simple problems. In particular the study of so-called diffusion flames – also known as non-premixed flames – requires special consideration. In a diffusion flame, the reactants are initially spatially separated. For this kind of system, mixing plays a crucial role because reactants need to be brought together to the flame zone in order to maintain combustion. Many practical applications of diffusion flames consider deflagration flames, Poinsot and Veynante, 2005 which are characterized by a small characteristic velocity compared to the speed of sound. The low-Mach approximation of the Navier–Stokes equations is often chosen for describing this kind of system. This approximation allows for the calculation of non-constant density flows (such as temperature dependent density), while neglecting acoustic effects, thus dramatically reducing the required temporal resolution. Müller, 1998

In addition to the compressibility effects mentioned above, the need to accurately and efficiently represent the chemical reactions governing the combustion problem poses a major challenge. Generally speaking, to study the combustion process a detailed chemistry description is preferable. However, this is often impractical as it can be very intensive computationally speaking. Stauch et al. investigated systems with detailed mechanism for methanol combustion, where 23 chemical species and 166 elementary reactions are involved, Stauch et al., 2006 and for n-heptane with 62 chemical species and 572 elementary reactions, and with detailed transport processesStauch and Maas, 2007. Because of their high complexity the mentioned works are restricted to simple one- or two-dimensional configurations, and to a small number of grid elements. If one is interested in more complex geometries or more complicated flow systems, the use of detailed kinetics can be prohibitive. Simplified kinetic models have been developed to overcome this difficulty. In the work of Westbrook et al. Westbrook and Dryer, 1981 a one-step kinetic model is presented, where combustion is expressed as a single chemical reaction with a reaction rate given by an Arrhenius-type expression with constant parameters. Multi-step chemical reaction models have also been developed, such as the four-step mechanism for methane combustion by Peters, Peters, 1985 or the three-step mechanism by Peters and Williams. Peters and Williams, 1987 Furthermore, extensions of one-step models exist, such as the one presented by Fernandez-Tarrazo et al. Fernandez-tarrazo et al., 2006 for hydrocarbon combustion with air, where kinetic parameters are correlated to the equivalence ratio in order to better describe characteristic flame properties for premixed and non-premixed flames.

In the last decades several numerical investigations related to diffusion flames have been carried out. Burke and Schumann were the first ones to investigate the structure of diffusion flames by studying the flame jet problem. Burke and Schumann, 1928 By assuming an infinitely

fast chemical reaction they managed to predict flame properties fairly accurately. In the work of Smooke et al. Smooke et al., 1986 a numerical simulation for a two-dimensional axisymmetric laminar diffusion jet with detailed chemistry was conducted and solved with Newton-type methods. In order to obtain adequate initial estimates for this problem, the solution of the problem for an infinitely fast chemistry was solved first. This idea was used in several works such as that by Keyes and Smooke Keyes and Smooke, 1987 for a counter diffusion flame, by Smooke Smooke and Giovangigli, 1992 for a Tsuji-counterflow configuration and in the work by Dobbins et al. Dobbins and Smooke, 2010 for an axisymmetric laminar jet diffusion flame with time dependent boundary conditions. In the work of Paxion Paxion et al., 2001 unstructured multigrid solver for laminar flames with detailed chemistry is presented. A Krylov-Newton method was used for solving several flame configurations. A two-dimensional counter diffusion flame was calculated, and its results were compared with the one-dimensional self-similar solution of the equations.

The DG method has also been used for simulations of combustion, mainly within a fully compressible framework. In the work from Johnson et al. Johnson and Kercher, 2020 the compressible Navier–Stokes equations are solved using a nodal DG scheme for combustion with complex chemistry and transport parameters. An hp-adaptive method is also presented, and shown to be useful for solving the ordinary differential equations used for describing the unsteady behaviour of the system. Similarly in the work from Lv and Ihme Lv and Ihme, 2017 a DG solver for multi-component chemically reacting flows, which solves the fully compressible Navier-Stokes equation, is presented. A hybrid-flux formulation is used, where a conservative Riemann solver is used for shock treatment, and a double-flux formulation is used in smooth regions. They show its applicability for non-reacting and reacting flows, particularly for systems characterized by high Mach numbers. On the other hand, the solution of combustion problems using the DG method in an incompressible framework is a topic that has not received much attention in the literature. This fact is the motivation of the present paper.

The system of equations obtained from the discretization of highly nonlinear systems can be very difficult to solve. Fixed-point iteration schemes have been used as a linearization strategy, as done by Klein et al. Klein et al., 2016 A major drawback of this approach is the highly problem dependent choice of under-relaxation factors. A much more robust strategy is the use of Newton type methods. Shadid et al., 1997; Pawlowski et al., 2006 Here, a problem-dependent factor is not needed. There is however a trade-off, because the Jacobian matrix has to be calculated, which can be computationally expensive. This approach has been used for combustion problems in numerous works. Karaa et al. Karaa et al., 2003 studied the axisymmetric laminar jet diffusion flame and investigated the behaviour of a multi-grid solver when using different pre-conditioners with a damped Newton algorithm. Shen et al. Shen et al., 2006 investigated the use and efficiency of a Newton method coupled with the Bi-CGSTAB method for an axisymmetric laminar jet flame. They concluded that, in terms of computational cost, the steady-state solution is more efficiently obtained by directly solving the steady formulation of the equations, than by solving the transient Navier-Stokes equations until the steady state is reached.

It is well known that the Newton method shows the property of having quadratic convergence sufficiently close to the solutionDeuflhard, 2011. However, if the initial solution guess is not adequate, the method converge to a solution slowly, or may not even converge at all. For some highly nonlinear problems this is a significant issue. The so-called globalized Newton methods are used to overcome this problem by effectively increasing the area of convergence of the method. A popular globalized Newton method is the Newton-Dogleg method, Pawlowski et al.,

2008 which is based on a trust-region technique.

In the present work, a steady low-Mach pressure-based solver for the simulation of temperature dependent non-reactive and reactive flows using the Discontinuous Galerkin method is presented. To the best of our knowledge, this is the first time that a pressure-based solver is used together with the DG method for solving the reactive low-Mach equations using the Newton-Dogleg method in a fully coupled manner. We focus in this study on two-dimensional configurations, but the ideas presented could be extended to three-dimensional systems. The one-step combustion model presented by Fernandez-Tarrazo et al. Fernandez-tarrazo et al., 2006 is used for describing the chemical reactions. In the present work we consider only methane combustion, but the one-step model could be used for other hydrocarbons as well. We choose this chemical model to obtain physically correct results for a wide range of applications, while avoiding the use of complex chemistry models. The discrete system of equations is solved by a globalized Newton method, by means of the Dogleg approach. In addition to the Newton-Dogleg method, a homotopy strategy is presented, which was found to be useful for obtaining solutions of steady state calculations of highly nonlinear problems. In order to find appropriate initial values for Newton's method in combustion applications, the concept of flame sheet estimates (i.e. the solution for infinitely fast chemistry) is used. Several benchmark cases are presented that allow us to validate our implementation. First we solve the differentially heated cavity problem, with which we intend to validate our implementation of the low-Mach solver for non-constant density flows using the fully coupled solver. Later two flame configurations are calculated, namely the counter-diffusion flame and the chambered diffusion flame. (Matalon et al., 1980)

In the following, we consider a two-dimensional system. However, the methods shown in this work could be also used for three-dimensional problems.

They were first derived by Rehm and Baum (Rehm and Baum, 1978). A rigorous extension to combustion problems was done by Majda and Sethian (Majda and Sethian, 1985).

2 Governing equations

In this work we present the methodology used to simulate reactive fluids in the low-Mach regime using the DG method. In this chapter we intend to show the governing equations, which will be discretized in the following chapters. First, in Section 2.1 the equations for a flow in the low-Mach regime with finite reaction velocity are shown. A brief derivation of the set low-Mach equations is presented, which should also serve as a way of showing and justifying the assumptions made in this work. We restricted ourselves to a one-step chemical model, but the algorithm presented could also be used for more complex chemistry models. Subsequently, in Section 2.2 the governing equations are shown for the case of assuming an irreversible chemical model with an infinite reaction rate. This case is often called the Burke–Schumann limit. These equations are used as part of the algorithm to solve the finite reaction rate case.

2.1 The low-Mach number equations for reactive flows

Combustion processes can be modeled by a system of nonlinear partial differential equations, namely the balance equations for total mass, momentum, energy, and mass of individual species (usually expressed in terms of mass fractions). This system needs to be solved together with an equation of state and expressions for the transport properties as well as for the chemical reaction rates. The derivation of the governing equations for a reacting flow system can be found in the literature. (see, for example, (Kee et al., 2003), (Poinsot and Veynante, 2005)). In the following pages, the main ideas regarding the derivation of equations are presented. For a more detailed explanation, we refer to the cited works and the references therein.

2.1.1 The reactive Navier–Stokes equations

Throughout this work, variables with a hat sign, e.g. $\hat{\rho}$ represent dimensional variables, while those without it are nondimensional. We start the derivation of the low-Mach number equations with the Navier–Stokes equations, the energy equation (in its temperature form), and the species transport equations. Let us consider a reacting fluid mixture composed of N species. Let $\hat{\mathbf{x}} = (\hat{x}, \hat{y}, \hat{z})$ and $\hat{t}$ be the spatial vector and time. The primitive variables are the velocity field $\hat{\mathbf{u}} = (\hat{u}, \hat{v}, \hat{w})$, the pressure $\hat{p}$, the temperature $\hat{T}$, and the mass fractions Y_k of the N total species. The set of governing equations to be solved is

$$\frac{\partial \hat{\rho}}{\partial \hat{t}} + \hat{\nabla} \cdot (\hat{\rho}\hat{\mathbf{u}}) = 0, \tag{2.1a}$$

$$\frac{\partial \hat{\rho}\hat{\mathbf{u}}}{\partial \hat{t}} + \hat{\nabla} \cdot (\hat{\rho}\hat{\mathbf{u}} \otimes \hat{\mathbf{u}}) = -\hat{\nabla}\hat{p} - \hat{\nabla} \cdot \hat{\tau} - \hat{\rho}\hat{\mathbf{g}}, \tag{2.1b}$$

$$\hat{\rho}\hat{c_p}\frac{\partial \hat{T}}{\partial \hat{t}} + \hat{\rho}\hat{c_p}\hat{\mathbf{u}} \cdot \hat{\nabla}\hat{T} = \frac{\mathrm{D}\hat{p}}{\mathrm{D}t} - \hat{\nabla} \cdot \hat{\mathbf{q}} + \hat{\tau} : \hat{\nabla}\hat{\mathbf{u}} + \hat{\omega}_T \tag{2.1c}$$

$$\frac{\partial \hat{\rho} Y_k}{\partial \hat{t}} + \hat{\nabla} \cdot (\hat{\rho}\hat{\mathbf{u}} Y_k) = -\hat{\nabla} \cdot \hat{\mathbf{j}_k} + \hat{\omega_k} \quad (k = 1, \ldots, N) \tag{2.1d}$$

This results in (in the general case) $N + 5$ differential equations to be solved. In these equations, $\hat{\rho}$ is the density of the mixture and $\hat{\mathbf{g}}$ is the acceleration of gravity. $\hat{\tau}$, $\hat{\mathbf{q}}$ and $\hat{\mathbf{j}}_k$ are the viscous tensor, the heat flux vector and the molecular mass flux vector of species k, respectively. Additionally, $\hat{\omega}_T$ is the heat release due to combustion and $\hat{\omega}_k$ is the reaction rate of species k. To close the system, expressions must be defined to link these variables with the primitive variables. They will be briefly shown and commented upon in the following paragraphs.

Equation of state

Assuming that the fluid behaves ideally, the density can be calculated as

$$\hat{\rho} = \frac{\hat{p}\hat{W}_{\text{avg}}}{\mathcal{R}\hat{T}}. \tag{2.2}$$

Here, $\hat{\mathcal{R}}$ is the universal gas constant of gases, and $\hat{W}_{\text{avg}}$ is the average molecular weight of the fluid, defined as

$$\hat{W}_{\text{avg}} = \left(\sum_{k=1}^{N} \frac{Y_k}{\hat{W}_k} \right)^{-1} \tag{2.3}$$

with $\hat{W}_k$ as the molecular weight of species k. For an ideal mixture, the specific heat capacity can be calculated as weighted averages of the specific heats of the species,

$$\hat{c}_p = \sum_{k=1}^{N} Y_k \hat{c}_{p,k}, \tag{2.4}$$

where $\hat{c}_{p,k}$ corresponds to the specific heat capacity of the component k. The temperature dependence of $\hat{c}_{p,k}$ can be accounted for by using NASA polynomials (Mcbride et al., 1993).

$$\hat{c}_{p,k} = \left(\hat{a}_1 + \hat{a}_2\hat{T} + \hat{a}_3\hat{T}^2 + \hat{a}_4\hat{T}^3 + \hat{a}_5\hat{T}^4 \right) \frac{\hat{\mathcal{R}}}{\hat{W}_k} \tag{2.5}$$

where $\hat{a}_1$, $\hat{a}_2$, $\hat{a}_3$, $\hat{a}_4$ and $\hat{a}_5$ are numerical coefficients supplied by the NASA database.

Transport models

The viscous tensor $\hat{\tau}$ is defined for a Newtonian fluid as

$$\hat{\tau} = -\hat{\mu}\left(\hat{\nabla}\hat{\mathbf{u}} + (\hat{\nabla}\hat{\mathbf{u}})^T \right) + \left(\frac{2}{3}\hat{\mu} - \hat{\kappa} \right) (\hat{\nabla} \cdot \hat{\mathbf{u}})\boldsymbol{I} \tag{2.6}$$

Here, $\hat{\mu}$ is the dynamic viscosity of the fluid, which is generally specific to the fluids and depends on its temperature and pressure. Furthermore, $\hat{\kappa}$ corresponds to the bulk viscosity, which is usually negligible for fluids at low pressures (Bird et al., 1960). $\hat{\kappa}$ will be taken equal to zero in the rest of this work.

The heat flux vector $\hat{\mathbf{q}}$ is given by Fourier's law of heat conduction,

$$\hat{\mathbf{q}} = \hat{\lambda}\hat{\nabla}\hat{T}. \tag{2.7}$$

Here $\hat{\lambda}$ corresponds to thermal conductivity, which, similar to the viscosity, is dependent on the particular fluid under study and its temperature and pressure.

The molecular mass flux vector $\hat{\mathbf{j}}_k$ of species k is defined as $\hat{\mathbf{j}}_k = \hat{\rho}\hat{\mathbf{U}}_k$. Here $\hat{\mathbf{U}}_k$ is the diffusion velocity of the component k. In general, $\hat{\mathbf{U}}_k$ can be obtained by solving the Maxwell-Stefan equations.

$$\nabla X_p = \sum_{k=1}^{N} \frac{X_p X_k}{D_{pk}} (\mathbf{U}_k - \mathbf{U}_p) \qquad p = 1, \ldots, N. \tag{2.8}$$

Here $D_{pk} = D_{kp}$ is the binary mass diffusion coefficient of species p in species k. X_p is the mole fraction of species k and is related to the mass fraction of k as $X_k = Y_k \hat{W}/\hat{W}_k$. The solution of the system (2.8) is often a difficult and costly task (Williams, 2000; Poinsot and Veynante, 2005), and often simplifications are made. It can be shown that for binary mixtures ($N = 2$) and for mixtures containing multiple species ($N > 2$) where all diffusion coefficients are equal, the system (2.8) reduces exactly to the well-known Fick's law.

$$\hat{\mathbf{j}}_k = -\rho \hat{D}_k \nabla Y_k \tag{2.9}$$

This expression is only exact in the cases mentioned above. For a system where the heat capacities of each species are different, this expression is inconsistent. The variable $\hat{D}_k$ corresponds in this case to the diffusion coefficient of species k in the mixture. An issue regarding the global mass conservation can be pointed out here. Recall that by definition the sum of the the mass fractions must always be one ($\sum_k^N Y_k = 1$). This is only true for the solution of Equation (2.1) if exact expressions for the diffusion velocities are used (Poinsot and Veynante, 2005). If some inexact expression is used (as for example Fick's law), the constraint for the sum of the mass fractions will not be fulfilled. This problem can be surpassed by solving the global mass conservation (continuity) equation Equation (2.1a) and only the equations for the first $N - 1$ species Equation (2.1d). Therefore, all inconsistencies that originated from not using an exact species diffusion model are absorbed by Y_N. As pointed out in Poinsot and Veynante, 2005, this simplification should only be used if all $N - 1$ species are strongly diluted in species N, such as the case of a flame in air, where the mass fraction of nitrogen is large. It can also be noted that this approach reduces in one the number of differential equations needed to be solved.

The temperature dependence of viscosity can be modeled by Sutherland's law (Sutherland, 1893)

$$\hat{\mu}(\hat{T}) = \hat{\mu}_{\text{suth}} \left(\frac{\hat{T}}{\hat{T}_{\text{suth}}} \right)^{1.5} \frac{\hat{T}_{\text{suth}} + \hat{S}}{\hat{T} + \hat{S}}. \tag{2.10}$$

Here $\hat{\mu}_{\text{suth}}$ is the viscosity evaluated at a reference temperature $\hat{T}_{\text{suth}}$, and $\hat{S}$ is a material dependent parameter. In all calculations in this work the value of $\hat{S}$ for air is used, $\hat{S} = 110.5\,\text{K}$. Expressions for determining the thermal conductivity and diffusion coefficients as function of temperature can be obtained using similar expressions, as will be shown later in Section 2.1.2

Chemical model

Consider a system composed of N species where M chemical reactions take place. Chemical reactions can be written in generalized form as follows.

$$\sum_{k=1}^{N} \nu'_{kj} \mathcal{M}_k \rightleftharpoons \sum_{k=1}^{N} \nu''_{kj} \mathcal{M}_k \qquad \text{for} \qquad j = 1, \ldots, M \tag{2.11}$$

where ν'_{jk} and ν''_{jk} are the molar stoichiometric coefficients of species k in the chemical reaction j, and $\mathcal{M}_j$ represents the chemical component k.

The reaction rate of species k is $\hat{\omega}_k$, which accounts for the total amount of species k that appear or disappear due to M chemical reactions (c.f. Equations (2.11)). Its given by

$$\hat{\omega}_k = \hat{W}_k \sum_{j=1}^{M} \nu_{jk} \hat{\mathcal{Q}}_j. \tag{2.12}$$

Here $\nu_{kj} = \nu''_{kj} - \nu'_{kj}$, and $\mathcal{Q}_j$ is the rate of progress of the reaction j. They are usually modeled using Arrhenius-type expressions, as will be shown later.

The heat release $\hat{\omega}_T$ that appears in the energy equation is related to the reaction rates according to

$$\hat{\omega}_T = -\sum_{k=1}^{N} \hat{h}_k \hat{\omega}_k = -\sum_{k=1}^{N} \Delta \hat{h}^0_k \hat{\omega}_k - \sum_{k=1}^{N} \hat{h}_{ks} \hat{\omega}_k \tag{2.13}$$

Here, the specific enthalpy of k-th species $\hat{h}_k$ is written in terms of its formation enthalpy $\hat{h}^0_k$ and a sensible enthalpy $\hat{h}_{ks} = \int_0^{\hat{T}} \hat{c}_{p,k} \mathrm{d}\hat{T}$. The second term on the right-hand side of Equation (2.13) is usually small and is exactly zero for a mixture where all the heat capacities of each component are equal (Poinsot and Veynante, 2005). It will be neglected in the rest of the analysis.

In this work, we use the one-step kinetic model for the combustion of hydrocarbons presented in Fernandez-tarrazo et al., 2006. The chemical reaction is represented by a single ($M = 1$) exothermic global irreversible expression as

$$\mathrm{C}_n\mathrm{H}_m + \left(n + \frac{m}{4}\right) \mathrm{O}_2 \longrightarrow n\mathrm{CO}_2 + \frac{m}{2}\mathrm{H}_2\mathrm{O} \tag{2.14}$$

The rate of progress of the global reaction is modeled by an Arrhenius-type expression

$$\hat{\mathcal{Q}} = \hat{B} e^{-\hat{T}_a/\hat{T}} \left(\frac{\hat{\rho} Y_F}{\hat{W}_F}\right)^a \left(\frac{\hat{\rho} Y_O}{\hat{W}_O}\right)^b. \tag{2.15}$$

Here, the subscripts F and O refer to fuel and oxidizer, respectively. The parameter $\hat{B}$ corresponds to the pre-exponential factor, $\hat{T}_a$ is the activation temperature, and a and b are reaction orders. For a one-step reaction model, the reaction rate of the k-th component (Equation (2.12)) is

$$\hat{\omega}_k = \nu_k \hat{W}_k \hat{\mathcal{Q}}. \tag{2.16}$$

With this definition, the heat release $\hat{\omega}_T$ (Equation (2.13)) is

$$\hat{\omega}_T = -\hat{W}_F \hat{\omega}_F \hat{Q}^m. \tag{2.17}$$

Here is $\hat{Q}^m$ the molar heat of reaction of the one-step reaction. $\hat{W}_F$ and $\hat{\omega}_F$ are the molar mass of the fuel species and the reaction rate of the fuel species.

Within the model from (Fernandez-tarrazo et al., 2006), several parameters are adjusted to represent characteristic features of premixed flames and diffusion flames. The parameters $\hat{T}_a$

$\hat{B}$ $(\mathrm{cm}^3/(\mathrm{mol\,s}))$	$\hat{T}_{a0}$ (K)	$\hat{\mathrm{Q}}_0$ $(\mathrm{MJ\,kmol}^{-1})$	a	b
6.9×10^{14}	15 900	802.4	1	1

Table 2.1: Base parameters used in the one-step combustion model by Fernandez-tarrazo et al., 2006

and $\hat{\mathrm{Q}}$ are defined as functions of the local equivalence ratio ϕ, which is, in turn, defined in terms of the local mass fractions of fuel Y_F and oxidizer Y_O as

$$\phi = \frac{sY_F^0}{Y_O^0} \frac{sY_F - Y_O + Y_O^0}{s(Y_F^0 - Y_F) + Y_O}, \tag{2.18}$$

where Y_F^0 and Y_O^0 are the mass fractions of the fuel and oxidizer flows in their corresponding feed streams, and s is the mass stoichiometric ratio, defined as $s = \nu_O \hat{W}_O / \nu_F \hat{W}_F$. The activation energy and molar heat release depend on ϕ as

$$\hat{T}_a(\phi) = \begin{cases} (1 + 8.250(\phi - 0.64)^2)\hat{T}_{a0} & \text{if } \phi \leq 0.64, \\ \hat{T}_{a0} & \text{if } 0.64 \leq \phi \leq 1.07, \\ (1 + 4.443(\phi - 1.07)^2)\hat{T}_{a0} & \text{if } \phi \geq 1.07, \end{cases} \tag{2.19}$$

$$\hat{\mathrm{Q}}(\phi) = \begin{cases} \hat{\mathrm{Q}}_0 & \text{if } \phi \leq 1 \\ (1 - \alpha(\phi - 1))\hat{\mathrm{Q}}_0 & \text{if } \phi > 1, \end{cases} \tag{2.20}$$

The parameter α is a constant that depends on the hydrocarbon being considered. In particular $\alpha = 0.21$ for the combustion of methane.

2.1.2 The unsteady non-dimensional low-Mach equations

In the present work, we use the low-Mach number equation approximation of the governing equations. The derivation of the equations can be found in (**mullerLowMachNumberAsymptoticsNavierStoke** Rehm and Baum, 1978; Majda and Sethian, 1985). We refer to these references for a detailed explanation on how the set of equations is derived. In the following, we restrict ourselves to show and comment on the main consequences of the low-Mach limit.

The low-Mach number limit approximation of the governing equations is used for flows where the Mach number (defined as $\mathrm{Ma} = \hat{u}_{\mathrm{ref}}/\hat{c}$, where $\hat{u}_{\mathrm{ref}}$ is a characteristic flow velocity and $\hat{c}$ the speed of sound) is small, which is usually the case in typical laminar combustion systems. (Dobbins and Smooke, 2010). The low-Mach equations are obtained by using standard asymptotic methods. One of the main results of the analysis is that for flows with a small Mach number, the pressure can be decomposed as

$$\hat{p}(\hat{\mathbf{x}}, \hat{t}) = \hat{p}_0(\hat{t}) + \hat{p}_2(\hat{\mathbf{x}}, \hat{t}). \tag{2.21}$$

The spatially uniform term $\hat{p}_0(\hat{t})$ is called thermodynamic pressure, and only appears in the equation of state. It is constant in space, but can change in time. For an open system, the thermodynamic pressure is constant and equal to the ambient pressure, while for a closed system (e.g. a system completely bounded by walls) it changes in order to ensure mass conservation.On the other hand, the perturbational term $\hat{p}_2(\hat{\mathbf{x}}, \hat{t})$ appears only in the momentum equations

and plays a role similar to that of the pressure in the classical incompressible formulation. This perturbational term satisfies $\hat{p}_2/\hat{p} \sim \mathcal{O}(\mathrm{Ma})^2$, (Dobbins and Smooke, 2010; Nonaka et al., 2018) showing that under these assumptions, the equation of state is satisfied only to $\mathcal{O}(\mathrm{Ma}^2)$ (cf. Equation (2.2))

Effectively, the low-Mach limit of the Navier-Stokes equations allows for the calculation of systems where big density variations due to temperature differences are present, thus not restricting ourselves to approximations such as the Boussinesq approximation for bouyancy-driven flow. In addition, this approximation truncates the mechanism of pressure wave propagation which is a natural feature of the compressible Navier-Stokes equations. In doing this, we are no longer restricted to choosing small timesteps to be able to resolve wave phenomena, and the maximum allowed timestep is greatly increased. From now on we will drop the sub-index of the hydrodynamic pressure $\hat{p}_2$ and we will refer to it simply as $\hat{p}$, further emphasizing the similarity in its role to the pressure of the incomprehensible formula.

In this work we use a non-dimensional formulation of the governing equations. We define the non-dimensional quantities.

$$\rho = \frac{\hat{\rho}}{\hat{\rho}_{\text{ref}}}, \quad p = \frac{\hat{p}}{\hat{p}_{\text{ref}}}, \quad \mathbf{u} = \frac{\hat{\mathbf{u}}}{\hat{u}_{\text{ref}}}, \quad T = \frac{\hat{T}}{\hat{T}_{\text{ref}}}, \quad c_p = \frac{\hat{c}_p}{\hat{c}_{p,\text{ref}}}, \quad W_k = \frac{\hat{W}_k}{\hat{W}_{\text{ref}}}$$
$$\mu = \frac{\hat{\mu}}{\hat{\mu}_{\text{ref}}}, \quad D_k = \frac{\hat{D}_k}{\hat{D}_{k,\text{ref}}}, \quad k = \frac{\hat{k}}{\hat{k}_{\text{ref}}} \quad \nabla = \frac{\hat{\nabla}}{\hat{L}_{\text{ref}}}, \quad t = \frac{\hat{t}}{\hat{t}_{\text{ref}}}, \quad \mathbf{g} = \frac{\hat{\mathbf{g}}}{\hat{g}_{\text{ref}}}, \quad Q = \frac{\hat{Q}}{\hat{Q}_0}$$

Here $\hat{u}_{\text{ref}}$, $\hat{L}_{\text{ref}}$, $\hat{p}_{\text{ref}}$, $\hat{t}_{\text{ref}}$, and $\hat{T}_{\text{ref}}$ are the reference velocity, length, pressure, time, and temperature, respectively, and are equal to some characteristic value for the particular configuration studied. Furthermore, $\hat{g}_{\text{ref}}$ is the magnitude of the gravitational acceleration and $\hat{W}_{\text{ref}}$ is the reference molecular weight. The reference transport properties $\hat{\mu}_{\text{ref}}$, $\hat{k}_{\text{ref}}$, $\hat{D}_{k,\text{ref}}$ and the reference heat capacity of the mixture and $\hat{c}_{p,\text{ref}}$ are evaluated at the reference temperature $\hat{T}_{\text{ref}}$. Similarly, the reference density must satisfy the equation of state, thus $\hat{\rho}_{\text{ref}} = \hat{p}_{\text{ref}}/(\hat{\mathcal{R}}\hat{T}_{\text{ref}}\hat{W}_{\text{ref}})$. By introducing these definitions into the governing equations (Equations (2.1a) to (2.1d)) the reactive set of non-dimensional low-Mach number equations is obtained. The system of differential equations to be solved reads as follows.

$$\frac{\partial \rho}{\partial t} + \nabla \cdot (\rho \mathbf{u}) = 0, \tag{2.22a}$$
$$\frac{\partial \rho \mathbf{u}}{\partial t} + \nabla \cdot (\rho \mathbf{u} \otimes \mathbf{u}) = -\nabla p + \frac{1}{\mathrm{Re}} \nabla \cdot \mu \left(\nabla \mathbf{u} + \nabla \mathbf{u}^T - \frac{2}{3} (\nabla \cdot \mathbf{u}) \boldsymbol{I} \right) - \frac{1}{\mathrm{Fr}^2} \rho \mathbf{g}, \tag{2.22b}$$
$$\frac{\partial \rho T}{\partial t} + \nabla \cdot (\rho \mathbf{u} T) = \frac{1}{\mathrm{Re\ Pr}} \nabla \cdot \left(\frac{k}{c_p} \nabla T \right) + \mathrm{H\ Da}\ \frac{\mathrm{Q}\ \mathcal{Q}}{c_p}, \tag{2.22c}$$
$$\frac{\partial \rho Y_k}{\partial t} + \nabla \cdot (\rho \mathbf{u} Y_k) = \frac{1}{\mathrm{Re\ Pr\ Le}_k} \nabla \cdot (\rho D \nabla Y_k) + \mathrm{Da}\ \nu_k W_k \mathcal{Q}. \quad (k = 1, \ldots, N-1) \tag{2.22d}$$

Note that we assumed that the spatial gradients of the mixture heat capacity are small, allowing us to introduce it in the derivative of the diffusive term of Equation (2.22c). Furthermore, using the fact that the sum of the mass fractions must always be one, the mass fraction of the last species N can be calculated with

$$Y_N = 1 - \sum_{k=1}^{N-1} Y_k. \tag{2.23}$$

The N-th component mass fraction Y_N is calculated using Equation (2.23). This system is solved for the primitive variables velocity $\mathbf{u} = (u_x, u_y)$, pressure p, temperature T and mass fractions $\mathbf{Y} = (Y_1, \ldots, Y_N)$. We note that the form of the low-Mach equations is very similar to the Navier-Stokes equations. The greatest difference is in the decomposition of the pressure, as mentioned above. This similarity is beneficial, as it allows the use of similar techniques to solve the PDE system to those used for the completely incompressible case (Keshtiban et al., 2003).

Six non-dimensional factors arise from the non-dimensionalization process:

$$\mathrm{Re} = \frac{\hat{\rho}_{\mathrm{ref}}\hat{u}_{\mathrm{ref}}\hat{L}_{\mathrm{ref}}}{\hat{\mu}_{\mathrm{ref}}}, \quad \mathrm{Fr} = \frac{\hat{u}_{\mathrm{ref}}}{\sqrt{\hat{g}_{\mathrm{ref}}\hat{L}_{\mathrm{ref}}}}, \quad \mathrm{Pr} = \frac{\hat{c}_{p,\mathrm{ref}}\hat{\mu}_{\mathrm{ref}}}{\hat{k}_{\mathrm{ref}}},$$

$$\mathrm{Le}_k = \frac{\hat{k}_{\mathrm{ref}}}{\hat{\rho}_{\mathrm{ref}}\hat{D}_{k,\mathrm{ref}}\hat{c}_{p,\mathrm{ref}}}, \quad \mathrm{Da} = \frac{\hat{B}\hat{L}_{\mathrm{ref}}\hat{\rho}_{\mathrm{ref}}}{\hat{M}_{\mathrm{ref}}\hat{u}_{\mathrm{ref}}}, \quad \mathrm{H} = \frac{\hat{\mathrm{Q}}_0}{\hat{c}_{p,\mathrm{ref}}\hat{T}_{\mathrm{ref}}}$$

The first three equations define the Reynolds, Froude and Prandtl number respectively. Le_k is the Lewis number of species k. Finally Da and H are the Damköhler number and the non-dimensional heat release respectively. The non-dimensional progress of the global reaction reads as follows.

$$\mathcal{Q}(T, \mathbf{Y}) = \left(\frac{\rho Y_F}{M_F}\right)\left(\frac{\rho Y_O}{M_O}\right)\exp\left(\frac{-T_a}{T}\right), \tag{2.24}$$

where $T_a = \hat{T}_a/\hat{T}_{\mathrm{ref}}$. Furthermore, the non-dimensional heat release is

$$\mathrm{Q}(\phi) = \begin{cases} 1 & \text{if } \phi \leq 1 \\ (1 - \alpha(\phi - 1)) & \text{if } \phi > 1, \end{cases} \tag{2.25}$$

with ϕ evaluated according to Equation (2.18). In the low-Mach limit, the ideal gas equation depends on the thermodynamic pressure, temperature and mass fractions. It reads in its non-dimensional form

$$\rho(p_0, T, \mathbf{Y}) = \frac{p_0}{T\sum_{k=1}^{N}\frac{Y_k}{W_k}}. \tag{2.26}$$

As mentioned above, the thermodynamic pressure of a closed system is a parameter that has to be determined (for an open system is equal to the atmospheric pressure). Defining the initial mass of the fluid inside the closed system as m_0, and by integrating Equation (2.26) on the whole domain Ω, one obtains

$$p_0(T, \mathbf{Y}) == \frac{m_0}{\int_\Omega \frac{W_{\mathrm{avg}}}{T}\mathrm{d}V}, \tag{2.27}$$

Similarly, the non-dimensional specific heat capacity of the mixture c_p is calculated as

$$c_p(T, \mathbf{Y}) = \sum_{k=1}^{N} Y_k c_{p,\alpha}(T), \tag{2.28}$$

and the non-dimensional viscosity as

$$\mu(T) = T^{\frac{3}{2}}\frac{1 + \hat{S}}{\hat{T}_{\mathrm{ref}}T + \hat{S}}. \tag{2.29}$$

As mentioned before, the model for the transport parameters can be simplified by assuming constant values for the Prandtl and Lewis numbers. (Smoke and Giovangigli, 1991) and we can write $\mu(T) = k/c_p(T) = \rho D_k(T)$.

2.2 The flame sheet approximation

Here we introduce the concept of the flame sheet approximation, which is used in our solution algorithm for solving the finite reaction rate system given by Equations (2.1a), (2.1b), (2.22c) and (2.22d). We follow the ideas proposed in the work from Keyes and Smooke, 1987. Assuming that all species have the same constant heat capacity c_p and mass diffusion coefficient $D_k = D$, that the Lewis number is unity for all species, and that combustion can be described by a single-step chemical reaction, it is possible to obtain an equation for a scalar without source terms, taking a linear combination of the energy Equation (2.22c) and mass fraction Equation (2.22d). A commonly used scalar is the mixture fraction z, which per definition is equal to unity in the fuel feed stream, and equal to zero in the oxidizer feed stream. Thus, the system of Equations (2.1a), (2.1b), (2.22c) and (2.22d) can be simplified to solving the low-Mach Navier-Stokes equations together with an equation for the passive scalar z:

$$\frac{\partial \rho}{\partial t} + \nabla \cdot (\rho \mathbf{u}) = 0, \tag{2.30a}$$

$$\frac{\partial \rho \mathbf{u}}{\partial t} + \nabla \cdot (\rho \mathbf{u} \otimes \mathbf{u}) = -\nabla p + \frac{1}{\mathrm{Re}} \nabla \cdot \mu \left(\nabla \mathbf{u} + \nabla \mathbf{u}^T - \frac{2}{3} (\nabla \cdot \mathbf{u}) \boldsymbol{I} \right) - \frac{1}{\mathrm{Fr}^2} \rho \mathbf{g}, \tag{2.30b}$$

$$\frac{\partial \rho z}{\partial t} + \nabla \cdot (\rho \mathbf{u} z) = \frac{1}{\mathrm{Re\ Pr}} \nabla \cdot (\rho D \nabla z), \tag{2.30c}$$

which are solved together with the equation of state and expressions for the transport parameters. Note that the system is not closed, because ρ, μ and ρD are still functions of temperature and mass fractions. These fields can be related to the mixture fraction using the concept of the Burke-Schumann flame structure. (Burke and Schumann, 1928) In the case of an infinitely fast chemical reaction, fuel and oxidizer cannot co-exist. On one side of this sheet only oxidizer is found, and on the other side only fuel. The exact position of the flame sheet can be determined by finding the location of points where both reactant mass fractions Y_F and Y_O meet in stoichiometric proportions, that is, the points where the mixture fraction $z = z_{st}$, with

$$z_{st} = \frac{Y_O^0}{Y_O^0 + s Y_F^0}, \tag{2.31}$$

where Y_O^0 is the mass fraction of oxidizer in the oxidizer inlet stream, and Y_F^0 is the mass fraction of fuel in the fuel inlet stream. The Burke-Schumann solution provides analytical expressions for temperature and mass fraction fields on either side of the flame sheet as function of the mixture fraction z (see for example the textbook from Poinsot and Veynante, 2005 or the work from Keyes and Smooke, 1987).

$$T(z) = \begin{cases} z T_F^0 + (1-z) T_O^0 + \dfrac{Q Y_F^0}{c_p} z_{st} \dfrac{1-z}{1-z_{st}} & \text{if} \quad z \geq z_{st} \\ z T_F^0 + (1-z) T_O^0 + \dfrac{Q Y_F^0}{c_p} z & \text{if} \quad z < z_{st} \end{cases} \tag{2.32}$$

The mass fraction field of fuel and oxidizer species at either side of the flame are given by:

$$Y_F(z) = \begin{cases} Y_F^0 \dfrac{z - z_{st}}{1 - z_{st}} & \text{if} \quad z \geq z_{st} \\ 0 & \text{if} \quad z < z_{st} \end{cases} \tag{2.33}$$

$$Y_O(z) = \begin{cases} 0 & \text{if} \quad z \geq z_{st} \\ Y_O^0 \left(1 - \dfrac{z}{z_{st}}\right) & \text{if} \quad z < z_{st} \end{cases} \tag{2.34}$$

and finally, the mass fraction field of product species P is:

$$Y_P(z) = \begin{cases} Y_O^0 \dfrac{W_P \nu_P}{W_O \nu_O}(1 - z) & \text{if} \quad z \geq z_{st} \\ Y_F^0 \dfrac{W_P \nu_P}{W_F \nu_F} z & \text{if} \quad z < z_{st} \end{cases} \tag{2.35}$$

Once the mixture fraction field z is obtained, the temperature and mass fraction fields are uniquely defined by Equations (2.32) to (2.35), which are used to evaluate the density and the transport properties. This coupling between variables and the associated nonlinear system leads to the need for an iterative solution scheme.

The main idea of introducing this additional system (Equations (2.30a) to (2.30c)) is to find an approximate solution to the system where a finite reaction-rate is used (Equations (2.22a) to (2.22d)). In Figure 2.1 temperature and fuel mass fraction fields across the center-line of a counterflow flame configuration is shown. Clearly, both solutions are very similar, differing only in the area near the flame. However, this similarity is only valid under the assumptions made to derive Equation (2.30c). In the case that the Lewis number is not equal to one, or that the heat capacities are not equal for each species, the finite-rate solution will differ slightly from that obtained with the infinite-reaction rate.

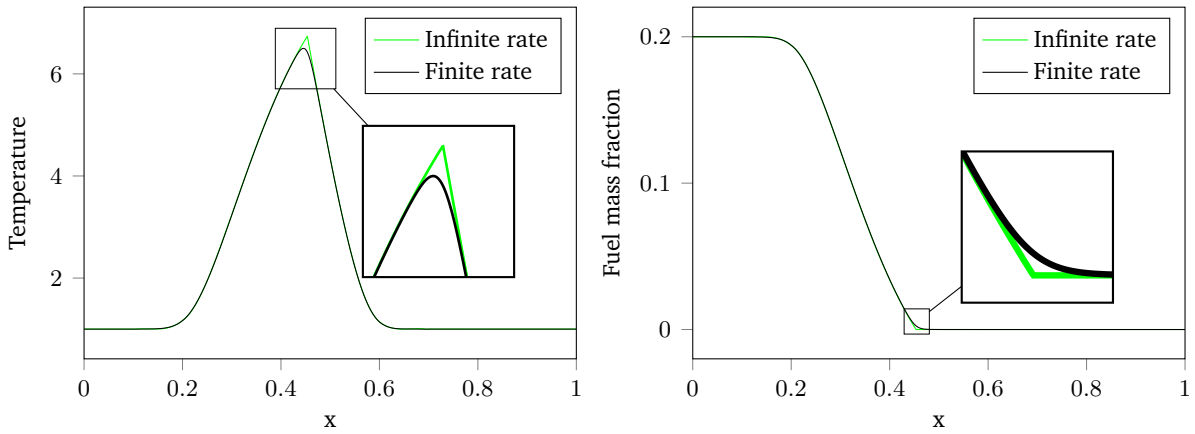

Figure 2.1: Temperature and fuel mass fraction profiles calculated in the center-line of a counter-flow flame configuration using finite chemistry (black) and the flame sheet approximation (green).

2.3 Boundary conditions

The following boundary conditions are imposed for the resolution of the finite reaction rate system (Equations (2.22a) to (2.22d)) and for the flame sheet problem (Equations (2.30a) to (2.30c)).

$$\Gamma_{\mathrm{D}}: \quad \mathbf{u} = \mathbf{u}_{\mathrm{D}}, \;\; T = T_{\mathrm{D}}, \;\; Y_k, = Y_{k,\mathrm{D}}, \;\; z = z_{\mathrm{D}}, \tag{2.36a}$$

$$\Gamma_{\mathrm{DW}}: \quad \mathbf{u} = \mathbf{u}_{\mathrm{D}}, \;\; \nabla T \cdot \mathbf{n}_{\partial\Omega} = 0, \;\; \nabla Y_k \cdot \mathbf{n}_{\partial\Omega} = 0, \;\; \nabla z \cdot \mathbf{n}_{\partial\Omega} = 0, \tag{2.36b}$$

$$\Gamma_{\mathrm{N}}: \quad \left(-p\mathbf{I} + \left(\frac{\mu}{\mathrm{Re}}\left(\nabla\mathbf{u} + (\nabla\mathbf{u})^T\right) - \frac{2}{3}\mu(\nabla\cdot\mathbf{u})\mathbf{I}\right)\right)\cdot\mathbf{n}_{\partial\Omega} = 0,$$
$$\nabla T \cdot \mathbf{n}_{\partial\Omega} = 0, \;\; \nabla Y_k \cdot \mathbf{n}_{\partial\Omega} = 0, \;\; \nabla z \cdot \mathbf{n}_{\partial\Omega} = 0, \tag{2.36c}$$

$$\Gamma_{\mathrm{ND}}: \quad \left(-p\mathbf{I} + \left(\frac{\mu}{\mathrm{Re}}\left(\nabla\mathbf{u} + (\nabla\mathbf{u})^T\right) - \frac{2}{3}\mu(\nabla\cdot\mathbf{u})\mathbf{I}\right)\right)\cdot\mathbf{n}_{\partial\Omega} = 0,$$
$$T = T_{\mathrm{D}}, \;\; Y_k = Y_{k,\mathrm{D}}, \;\; z = z_{\mathrm{D}} \tag{2.36d}$$

$$\Gamma_P: \quad \mathbf{u}(\mathbf{x}) = \mathbf{u}(\mathbf{x}'), \;\; T(\mathbf{x}) = T(\mathbf{x}'), \;\; Y_k(\mathbf{x}) = Y_k(\mathbf{x}'), \;\; z(\mathbf{x}) = z(\mathbf{x}'), \tag{2.36e}$$

where k denotes the index from mass fractions $k = (1, \ldots, N-1)$. The boundary Γ_{D} represents conditions for inlets and walls, with velocity, temperature, mass fractions and mixture fraction defined as Dirichlet boundary conditions. Boundaries Γ_{DW} are used to represent adiabatic walls, where velocity is given as a Dirichlet boundary condition, but with the gradients perpendicular to the wall of the transported scalars set to zero. The boundary Γ_{N} represent an outflow of the domain with homogeneous Neumann condition for all scalars. The boundary Γ_{ND} also represents an outlet boundary condition, but with Dirichlet boundary conditions for the scalars. Finally the boundaries Γ_P are periodic boundaries, where $\mathbf{x}$ and $\mathbf{x}'$ are periodic pairs in the domain.

3 Numerical methods

3.1 The Discontinous Galerkin method

3.1.1 Spatial discretization

We start by introducing some standard definitions and notations in the context of DG methods:Kummer, 2017 Kikker et al., 2020 We define a computational domain $\Omega \subset \mathbb{R}^2$ with a polygonal and simply connected boundary $\partial\Omega$. Our numerical grid is then defined by the set of non-overlapping elements $\mathcal{K} = \{K_1, ..., K_N\}$ with a characteristic mesh size h, so that Ω is the union of all elements, i.e. $\Omega = \bigcup_{i=1}^{N} K_i$. We define $\Gamma = \bigcup_j \partial K_j$ as the union of all edges (internal edges and boundary edges) and $\Gamma_I = \Gamma \setminus \partial\Omega$ as the union of all interior edges. For each edge of Γ a normal field $\mathbf{n}_\Gamma$ is defined. Particularly on $\partial\Omega$ is defined as an outer normal and $\mathbf{n}_\Gamma = \mathbf{n}_{\partial\Omega}$. For each field $\mathbf{u} \in C^0(\Omega \setminus \Gamma_I)$ we define $\mathbf{u}^-$ and $\mathbf{u}^+$, which describe the information in the interior and exterior sides of the cell:

$$\mathbf{u}^- = \lim_{\xi \searrow 0} \mathbf{u}(\mathbf{x} - \xi \mathbf{n}_\Gamma) \quad \text{for } \mathbf{x} \in \Gamma \tag{3.1}$$

$$\mathbf{u}^+ = \lim_{\xi \searrow 0} \mathbf{u}(\mathbf{x} + \xi \mathbf{n}_\Gamma) \quad \text{for } \mathbf{x} \in \Gamma_I \tag{3.2}$$

The jump and mean values of $\mathbf{u}$ on inner edges Γ_I are defined as:

$$[\![\mathbf{u}]\!] = \mathbf{u}^+ - \mathbf{u}^- \tag{3.3}$$

$$\{\mathbf{u}\} = \frac{1}{2}\left(\mathbf{u}^- + \mathbf{u}^+\right). \tag{3.4}$$

while the jump and mean values on boundary edges $\partial\Omega$ are:

$$[\![\mathbf{u}]\!] = \mathbf{u}^- \tag{3.5}$$

$$\{\mathbf{u}\} = \mathbf{u}^-. \tag{3.6}$$

We define the broken polynomial space of total degree k as

$$\mathbb{P}_k(\mathcal{K}_h) = \{f \in L^2(\Omega); \forall K \in \mathcal{K} : f|_K \text{ is polynomial and } \deg(f|_K) \leq k\}. \tag{3.7}$$

Additionally for $u \in \mathcal{C}^1(\Omega \setminus \Gamma)$ the broken gradient $\nabla_h u$ is defined as:

$$\nabla_h u = \begin{cases} 0 & \text{on } \Gamma \\ \nabla u & \text{elsewhere} \end{cases} \tag{3.8}$$

The broken divergence $\nabla_h \cdot u$ is defined analogously. Finally, we define the function space for test and trial functions for D_v dependent variables:

$$\mathbb{V}_{\mathbf{k}} = \prod_{i=1}^{D_v} \mathbb{P}_{k_i}(K_h) \tag{3.9}$$

where $\mathbf{k} = (k_1, ..., k_{D_v})$.

3.1.2 Discretization for a DG Method

As an introductory example, following **hesthaven_nodal_2008**, we are considering the discretization of a general conservation law with a non-linear flux function $\mathbf{f}(\psi)$ for a scalar quantity $\psi = \psi(\mathbf{x}, t)$ in Ω and suitable Dirichlet boundary condition on $\partial\Omega = \partial\Omega_\mathrm{D}$ and a compatible initial condition ψ_0. The problem statement reads

$$\frac{\partial \psi}{\partial t} + \nabla \cdot \mathbf{f}(\psi) = 0, \qquad \mathbf{x} \in \Omega, \tag{3.10a}$$

$$\psi = \psi_\mathrm{D}, \qquad \mathbf{x} \in \partial\Omega_\mathrm{D}, \tag{3.10b}$$

$$\psi(\mathbf{x}, 0) = \psi_0(\mathbf{x}), \qquad \mathbf{x} \in \Omega. \tag{3.10c}$$

The goal is to find an approximate solution $\psi = \psi(\mathbf{x}, t)$ to ψ that fulfils the problem (3.10). Therefore, the problem domain Ω is discretized by a numerical mesh $\mathfrak{K}_h$ and for each numerical cell K_j we introduce the approximation by a local polynomial basis $\boldsymbol{\phi}_j = (\phi_{j,l})_{l=1,\dots,N_k} \in \mathbb{P}_k(\{K_j\})$ with a cell-local support $\mathrm{supp}(\boldsymbol{\phi}_j) = \overline{K}_j$ as

$$\psi_j(\mathbf{x}, t) = \sum_{l=1}^{N_k} \tilde{\psi}_{j,l}(t)\phi_{j,l}(\mathbf{x}) = \tilde{\boldsymbol{\psi}}_j(t) \cdot \boldsymbol{\phi}_j(\mathbf{x}), \quad \mathbf{x} \in K_j, \tag{3.11}$$

where the coefficients $\tilde{\boldsymbol{\psi}}_j = (\tilde{\psi}_{j,l})_{l=1,\dots,N_k}$ denote the unknowns or degrees of freedom (DOF) of the local solution in cell K_j. In this work a modal polynomial basis is used, which fulfils the orthogonality condition

$$\int_{K_j} \phi_{j,m}\phi_{j,n} \,\mathrm{d}V = \delta_{mn} \tag{3.12}$$

with the Kronecker delta δ_{mn}. Inserting the local approximation (3.11) into the conservation law (3.10a) results in a cell-wise residual

$$R_j(\mathbf{x}, t) = \frac{\partial \psi_j}{\partial t} + \nabla \cdot \mathbf{f}(\psi_j), \quad \mathbf{x} \in K_j. \tag{3.13}$$

For a Galerkin method, the residual (3.13) is minimized with respect to the same space as the ansatz functions, i.e. $\mathbb{P}_k(\{K_j\})$. Thus, we demand for the test functions $\vartheta_{j,l} = \phi_{j,l}$ in each cell $K_j \in \mathfrak{K}_h$ that

$$\int_{K_j} R_j \vartheta_{j,l} \,\mathrm{d}V = \int_{K_j} \frac{\partial \psi_j}{\partial t}\phi_{j,l} + \nabla \cdot \mathbf{f}(\psi_j)\phi_{j,l} \,\mathrm{d}V \stackrel{!}{=} 0, \quad \forall \boldsymbol{\phi}_{j,l}. \tag{3.14}$$

So, for each cell we end up with a linear system of N_k equations. However so far, no approximate global solution $\psi \in \Omega$ can be regained from the minimization in (3.14). The global solution is assumed to be a piecewise polynomial approximation

$$\psi(\mathbf{x}, t) \approx \psi(\mathbf{x}, t) = \bigoplus_{j=1}^{J} \psi_j(\mathbf{x}, t) = \sum_{j=1}^{J}\sum_{l=1}^{N_k} \tilde{\psi}_{j,l}(t)\phi_{j,l}(\mathbf{x}) \in \mathbb{P}_k(\mathfrak{K}_h) \tag{3.15}$$

defined as the direct sum of the J local solutions ψ_j in (3.11). Here, $\tilde{\psi}_{j,l}$, with $j = 1, \dots, J$ and $l = 1, \dots, N_k$, denote the total DOF, with $N = J \cdot N_k$, of the global approximate solution ψ. In

order to formulate a global DG method, the spatial term on the right-hand side of equation (3.14) is rewritten in terms of boundary edge integrals $\forall K_j \in \mathfrak{K}_h$ using partial integration

$$\int_{K_j} \frac{\partial \psi_j}{\partial t} \phi_{j,l} \, \mathrm{d}V - \int_{K_j} \mathbf{f}(\psi_j) \cdot \nabla_h \phi_{j,l} \, \mathrm{d}V + \oint_{\partial K_j} \left(\mathbf{f}(\psi_j) \cdot \mathbf{n}_j \right) \phi_{j,l} \, \mathrm{d}S = 0, \quad \forall \phi_{j,l}, \tag{3.16}$$

where $\mathbf{n}_j$ represents the local outward pointing normal for cell K_j. Note that on the internal edges Γ_{int} the value of $\mathbf{f}(\psi_j)$ is multiply defined. Therefore, a numerical flux $\hat{F}$ is introduced

$$\hat{F}(\psi_j^{\text{in}}, \psi_j^{\text{out}}, \mathbf{n}_\Gamma) \approx \mathbf{f}(\psi_j) \cdot \mathbf{n}_j, \tag{3.17}$$

that uniquely defines the resulting value of both neighbouring values, i.e. ψ_j^{in} and ψ_j^{out} at internal edges Γ_{int}. Summing over all cells K_j, the global minimization problem for $\psi(\mathbf{x}, t), \mathbf{x} \in \Omega$ reads: Find $\psi \in \mathbb{P}_k(\mathfrak{K}_h)$, such that $\forall \vartheta = \phi \in \mathbb{P}_k(\mathfrak{K}_h)$

$$\int_\Omega \frac{\partial \psi}{\partial t} \phi \, \mathrm{d}V - \int_\Omega \mathbf{f}(\psi) \cdot \nabla_h \phi \, \mathrm{d}V + \oint_\Gamma \hat{F}(\psi^{\text{in}}, \psi^{\text{out}}, \mathbf{n}_\Gamma) \, [\![\phi]\!] \, \mathrm{d}S = 0, \tag{3.18}$$

where at Γ_{D} the outer value $\psi^{\text{out}} = \psi_{\text{D}}$ is given by the Dirichlet boundary condition (3.10b). In order to fully discretize the initial boundary value problem (3.10), one further needs to discretize the temporal term. This issue is skipped at this point and is discussed in Section **??**. Thus, the current form of (3.18) is referred to as the semi-discrete weak formulation of (3.10).

Considering the spatial discretization, the numerical flux $\hat{F}$ needs to satisfy certain mathematical and physical properties to ensure stability and convergence of the DG method. In this work the stability is defined in the continuous setting via the energy estimate

$$\|\psi(\mathbf{x}, t)\|_\Omega^2 \leq \|\psi(\mathbf{x}, 0)\|_\Omega^2, \quad \forall t \geq 0, \tag{3.19}$$

where homogenous Dirichlet conditions are assumed. Thus, stability is given, if the energy $\|\psi(\mathbf{x}, t)\|_\Omega^2$ only decreases in the absence of an inflow. Two properties need to be fulfilled in order to proof that the discrete problem (3.18) satisfies the discrete equivalent of the energy estimate in (3.19). The numerical flux $\hat{F}$ is required to be a function that is Lipschitz continuous and monotonic, see **di_pietro_mathematical_2012** for the proof. Furthermore, it is obvious that the DG method needs to regain a unique approximate solution to the underlying problem. Thus, $\hat{F}$ satisfies the following consistency property

$$\hat{F}(a, a, \mathbf{n}) = \mathbf{f}(a) \cdot \mathbf{n}, \quad \forall a \in \mathbb{R}. \tag{3.20}$$

A direct consequence of (3.20) is that the weak formulation (3.18) is directly fulfilled for $\psi = \psi$. Since considering a general conservation law in its conservative form, one further requires that $\hat{F}$ regains the global conservation property, i.e. the total amount of ψ only changes due to fluxes across the domain boundary $\partial\Omega$, by satisfying

$$\hat{F}(a, b, \mathbf{n}) = -\hat{F}(a, b, -\mathbf{n}), \quad \forall a, b \in \mathbb{R}. \tag{3.21}$$

The specific form of a suitable numerical flux $\hat{F}$ is presented in Section **??**, where the spatial discretization of the two-phase flow problem is discussed.

Note that the system (3.18) can be written in a shorten matrix formulation as

$$\mathbf{M} \frac{\mathrm{d}\tilde{\boldsymbol{\psi}}}{\mathrm{d}t} + \mathbf{Op}(\tilde{\boldsymbol{\psi}}) = \mathbf{b}, \tag{3.22}$$

where the sought-after coefficients are given as the solution vector $\tilde{\boldsymbol{\psi}} = \{\tilde{\psi}_{1,1}, \tilde{\psi}_{1,2}, ..., \tilde{\psi}_{j,n}, ..., \tilde{\psi}_{J,N_k}\} \in \mathbb{R}^N$. The mass matrix $\mathbf{M} \in \mathbb{R}^{N \times N}$ has a block-diagonal structure with

$$\mathbf{M} = \begin{bmatrix} \mathbf{M}_1 & 0 & \cdots & 0 \\ 0 & \mathbf{M}_2 & \cdots & 0 \\ \vdots & \vdots & \ddots & \vdots \\ 0 & 0 & \cdots & \mathbf{M}_J \end{bmatrix}, \tag{3.23}$$

where the cell-local mass matrix $\mathbf{M}_j$ is defined by

$$(\mathbf{M}_j)_{m,n} = \int_{K_j} \phi_{j,m}\phi_{j,n} \, \mathrm{d}V = \int_{K_j} \boldsymbol{\phi}_j \otimes \boldsymbol{\phi}_j \, \mathrm{d}V. \tag{3.24}$$

The cell-local Operator matrix $\mathbf{Op}_j$ is given by

$$(\mathbf{Op}_j)_{m,n} = -\int_{K_j} \mathbf{f}(\tilde{\psi}_{j,n}\phi_{j,n}) \cdot \nabla_h \phi_{j,m} \, \mathrm{d}V + \oint_{\partial K_j} \hat{F}(\tilde{\psi}_{j,n}, \tilde{\psi}_{j^*,n}, \mathbf{n}_\mathfrak{I})\phi_{j,m} \, \mathrm{d}S, \tag{3.25}$$

where j^* denotes the index of a neighbouring cell to K_j. Like the mass matrix, the operator matrix exhibits a block-diagonal structure, but including secondary diagonals due to the coupling with neighbouring cells over the numerical fluxes $\hat{F}$. The right-hand side $\mathbf{b}$ incorporates the given Dirichlet boundary condition value ψ_D.

Discontinuous Galerkin discretization of the finite reaction rate problem

We start by presenting the DG discretization of the finite reaction system defined by **??**–2.22d. We define $\mathbf{Y}' = (Y_1, \ldots, Y_{ns-1})$ as the vector containing the first $(n_s - 1)$ mass fractions and $\mathbf{s} = (s_1, \ldots, s_{ns-1})$ as the vector containing the test functions for the first $(n_s - 1)$ mass fraction equations. The discretized form of **????** and Equations (2.22c) and (2.22d) is obtained by multiplying each equation by a test function, integrating it over an element K, applying integration by parts and finally using an adequate numerical flux for each term. Note that the convective and diffusive terms of the temperature scalars T, mass fraction Y_α and mixture fraction z have the same form, so they share the same expression in their discretized form. In order to ensure the validity of the Ladyzenskaja-Babuška-Brezzi (or inf-sup) condition, Babuška, 1973 we use a mixed order formulation, where polynomials of order k for velocity, temperature and mass fractions, and of degree $k' = k - 1$ for pressure are used. Finally the discretized problem can be written as: find the numerical solution $(p_h, \mathbf{u}_h, T_h, \mathbf{Y}'_h) \in \mathbb{V}_\mathbf{k}$ such that for all test functions $(q_h, \mathbf{v}_h, r_h, \mathbf{s}_h) \in \mathbb{V}_\mathbf{k}$ we have:

$$\mathcal{C}\left(\mathbf{u}_h, q_h, \rho(T_h, \mathbf{Y}_h)\right) = \mathcal{B}^1(q_h), \tag{3.26a}$$

$$\mathcal{U}^C\left(\mathbf{u}_h, \mathbf{u}_h, \mathbf{v}_h, \rho(T_h, \mathbf{Y}_h)\right) + \mathcal{U}^P\left(p_h, \mathbf{v}_h\right) + \frac{1}{\mathrm{Re}}\mathcal{U}^D\left(\mathbf{u}_h, \mathbf{v}_h, \mu(T_h)\right) + \frac{1}{\mathrm{Fr}^2}\mathcal{U}^S\left(\rho(T_h, \mathbf{Y}_h), \mathbf{v}_h\right) = \mathcal{B}^2(\mathbf{v}_h), \tag{3.26b}$$

$$\mathcal{S}^C\left(\mathbf{u}_h, T_h, r_h, \rho(T_h, \mathbf{Y}_h)\right) + \frac{1}{\mathrm{Re\ Pr}}\mathcal{S}^D\left(T_h, r_h, k/c_p(T_h)\right) + \mathrm{H\ Da}\ \mathcal{S}^S\left(r_h, \mathrm{Q}(T_h, \mathbf{Y}_h), \omega(T_h, \mathbf{Y}_h), c_p(T_h, \mathbf{Y}_h)\right) = \mathcal{B}^3(r_h) \tag{3.26c}$$

$$\mathcal{S}^C\left(\mathbf{u}_h, Y_{\alpha h}, s_{\alpha h}, \rho(T_h, \mathbf{Y}_h)\right) + \frac{1}{\mathrm{Re\ Pr\ Le}_\alpha}\mathcal{S}^D\left(Y_{\alpha h}, s_{\alpha h}, \rho D_\alpha(T_h)\right) + \mathrm{Da}\mathcal{M}^S_\alpha\left(s_{\alpha h}, \omega(T_h, \mathbf{Y}_h)\right) = \mathcal{B}^3(s_{\alpha h}). \tag{3.26d}$$

where the index α takes values $\alpha = 1, \ldots, (n_s - 1)$. The n_s-th component mass fraction Y_{n_s} is calculated using Equation (2.23).

Discontinuous Galerkin discretization of the flame sheet problem

Discretizing the flame sheet problem given by Equations (2.30a) to (2.30c) proceeds in a similar way. Due to the similarity of the mass fraction equation and the mixture fraction equation the discretization is analogous. Again, we use a mixed order formulation of polynomials of degree k for velocity and mixture fraction, and of degree $k-1$ for pressure. The resulting problem reads: find the numerical solution $(p_h, \mathbf{u}_h, z_h) \in \mathbb{V}_\mathbf{k}$ such that for all test functions $(q_h, \mathbf{v}_h, r_h) \in \mathbb{V}_\mathbf{k}$ we have:

$$\mathcal{C}\left(\mathbf{u}_h, q_h, \rho(z_h)\right) = \mathcal{B}^1(q_h), \tag{3.27a}$$

$$\mathcal{U}^C\left(\mathbf{w}_h, \mathbf{u}_h, \mathbf{v}_h, \rho(z_h)\right) + \mathcal{U}^P\left(p_h, \mathbf{v}_h\right) + \frac{1}{\mathrm{Re}}\mathcal{U}^D\left(\mathbf{u}_h, \mathbf{v}_h, \mu(z_h)\right) + \frac{1}{\mathrm{Fr}^2}\mathcal{U}^S\left(\rho(z), \mathbf{v}_h\right) = \mathcal{B}^2(\mathbf{v}_h), \tag{3.27b}$$

$$S^C\left(\mathbf{u}_h, z_h, r_h, \rho(z_h)\right) + \frac{1}{\mathrm{Re}\,\mathrm{Pr}}\mathcal{S}^D\left(z_h, r_h, \rho D(z_h)\right) = \mathcal{B}^3(r_h). \tag{3.27c}$$

Note that density and transport parameters are dependent on the mixture fraction z. The evaluation of those parameters is done as mentioned in **??** and solved iteratively using a Newton-Dogleg type method as shown later in Section 3.2.1

Definitions of nonlinear forms

We show in the following the nonlinear forms used in this work. Regarding the choice of fluxes, we follow the "best practices" known in literature for the incompressible Navier-Stokes equation. It is known Pietro and Ern, 2012; Girault et al., 2004 that central difference fluxes for the pressure gradient and velocity divergence, combined with a coercive form for the viscous terms, e.g. symmetric interior penalty, gives a stable discretization for the Stokes equation. Furthermore, it is known that for all kinds of convective terms, a numerical flux which transports information in characteristic direction, e.g. Upwind, Lax-Friedrichs or Local-Lax-Friedrichs, must be used. We opted for the last one in our implementation, as it offers a good compromise between accuracy and stability.

Continuity equation We use a central difference flux for the discretization of the continuity equation:

$$\mathcal{C}(\mathbf{u}, q, \rho) = \oint_{\Gamma_\mathrm{I}\cup\Gamma_\mathrm{N}\cup\Gamma_\mathrm{ND}\cup\Gamma_\mathrm{P}} \{\rho\mathbf{u}\}\cdot\mathbf{n}_\Gamma \left[\!\left[q\right]\!\right] \,\mathrm{d}S - \int_\Omega \rho\mathbf{u}\cdot\nabla_h q \,\mathrm{d}V. \tag{3.28}$$

The density in Equation (3.28) is evaluated as a function of the temperature and mass fractions using the equation of state (Equation (2.26)). The term $\mathcal{B}^1$ on the right hand sides of Equation (3.26a) and Equation (3.27a) contains the Dirichlet boundary conditions:

$$\mathcal{B}^1(q) = -\oint_{\Gamma_\mathrm{D}\cup\Gamma_\mathrm{DW}} q(\rho_\mathrm{D}\mathbf{u}_\mathrm{D}\cdot\mathbf{n}_\Gamma).\,\mathrm{d}S \tag{3.29}$$

The density at the boundary ρ_D is evaluated with Equation (2.26) using the corresponding Dirichlet values of temperature and mass fractions.

Momentum equations The convective term of the momentum equations is discretized using a Lax-Friedrichs flux

$$\mathcal{U}^C(\mathbf{w},\mathbf{u},\mathbf{v},\rho) = \oint_\Gamma \left(\{\rho\mathbf{u}\otimes\mathbf{w}\}\,\mathbf{n}_\Gamma + \frac{\gamma_1}{2}[\![\mathbf{u}]\!]\right)\cdot[\![\mathbf{v}]\!]\,\mathrm{d}S - \int_\Omega(\rho\mathbf{u}\otimes\mathbf{w}):\nabla_h\mathbf{v}d\mathrm{V}. \tag{3.30}$$

The Lax-Friedrichs parameter γ_1 is calculated as Klein et al., 2016

$$\gamma_1 = \max\left\{2\overline{\rho^+}|\overline{\mathbf{u}^+}\cdot\mathbf{n}^+|, 2\overline{\rho^-}|\overline{\mathbf{u}^-}\cdot\mathbf{n}^-|\right\}, \tag{3.31}$$

where $\overline{\rho_h^\pm}$ and $\overline{\mathbf{u}^\pm}$ are the mean values of $\rho^\pm$ and $\mathbf{u}^\pm$ in $K^\pm$, respectively.
The pressure term is discretized by using a central difference flux

$$\mathcal{U}^P(p,\mathbf{v}) = \oint_{\Gamma\setminus\Gamma_\mathrm{N}\setminus\Gamma_\mathrm{ND}}\{p\}\,([\![\mathbf{v}]\!]\cdot\mathbf{n})\,\mathrm{d}S - \int_\Omega p\nabla_h\cdot\mathbf{v}\,\mathrm{d}V. \tag{3.32}$$

The diffusive term of the momentum equations is discretized using an Symmetric Interior Penalty (SIP) formulation Shahbazi, 2005

$$\begin{aligned}\mathcal{U}^D(\mathbf{u},\mathbf{v},\mu) = &\int_\Omega\left(\mu\left((\nabla_h\mathbf{u}) + (\nabla_h\mathbf{u})^T - \frac{2}{3}(\nabla_h\cdot\mathbf{u})\boldsymbol{I}\right)\right):\nabla_h\mathbf{v}\,\mathrm{d}V\\ &- \oint_{\Gamma\setminus\Gamma_\mathrm{N}\setminus\Gamma_\mathrm{ND}}\left(\left\{\mu(\nabla_h\mathbf{u}+\nabla_h\mathbf{u}^T - \frac{2}{3}(\nabla_h\cdot\mathbf{u})\boldsymbol{I})\right\}\mathbf{n}_\Gamma\right)\cdot[\![\mathbf{v}]\!]\,\mathrm{d}S\\ &- \oint_{\Gamma\setminus\Gamma_\mathrm{N}\setminus\Gamma_\mathrm{ND}}\left(\left\{\mu(\nabla_h\mathbf{v}+\nabla_h\mathbf{v}^T - \frac{2}{3}(\nabla_h\cdot\mathbf{v})\boldsymbol{I})\right\}\mathbf{n}_\Gamma\right)\cdot[\![\mathbf{u}]\!]\,\mathrm{d}S\\ &+ \oint_{\Gamma\setminus\Gamma_\mathrm{N}\setminus\Gamma_\mathrm{ND}}\eta\mu_{max}[\![\mathbf{u}]\!][\![\mathbf{v}]\!]\,\mathrm{d}S.\end{aligned} \tag{3.33}$$

The viscosity μ is evaluated as a function of temperature according to Equation (2.29) and $\mu_\mathrm{max} = \max(\mu^+,\mu^-)$. Additionally η is the penalty term of the SIP formulation, which has to be chosen big enough to ensure coercivity of the form, but also as small as possible in order to not increase the condition number of the problem. The estimation of the penalty term is based on an expression of the form

$$\eta = \eta_0\frac{A(\partial K)}{V(K)}, \tag{3.34}$$

where for a two-dimensional problem A is the perimeter and V the area of the element. Parameter η_0 is a safety factor and is set $\eta_0 = 4$ in all calculations. Further information on the determination of the penalty term can be found in **hillewaertDevelopmentDiscontinuousGalerkin2013b**.
The source term arising due to body forces is:

$$\mathcal{U}^S(\rho,\mathbf{v}) = \int_\Omega\rho\frac{\mathbf{g}}{\|\mathbf{g}\|}\cdot\mathbf{v}\,\mathrm{d}V. \tag{3.35}$$

The right hand sides of Equation (3.26b) and Equation (3.27b) contain the information from Dirichlet boundary conditions:

$$\mathcal{B}^2(\mathbf{v}) = -\oint_{\Gamma_\mathrm{D}}\left((\rho\mathbf{u}_\mathrm{D}\otimes\mathbf{u}_\mathrm{D})\mathbf{n}_\Gamma + \frac{\gamma_1}{2}\mathbf{u}_\mathrm{D}\right)\cdot\mathbf{v}\,\mathrm{d}S + \oint_{\Gamma_\mathrm{D}}\mu_\mathrm{D}\mathbf{u}_\mathrm{D}\cdot(\nabla_h\mathbf{v}\mathbf{n}_\Gamma + \nabla_h\mathbf{v}^T\mathbf{n}_\Gamma - \eta\mathbf{v})\,\mathrm{d}S. \tag{3.36}$$

The Dirichlet viscosity value μ_D is calculated from Equation (2.29) using the Dirichlet values of the temperature at the boundary.

Scalar equations Since the convective and diffusive term for the temperature, mass fractions and mixture fraction share a similar form, we summarize here their discretized expressions in terms of an arbitrary scalar X (corresponding to T in the energy equation, Y_α in the equation for species α and z for the mixture fraction equation) and transport parameter ξ (i.e. k/c_p in the energy equation, and (ρD) for the mass fraction and mixture fraction equations). The convective term of the scalars is discretized using a Lax-Friedrichs flux

$$\mathcal{S}^C(\mathbf{u}, X, r, \rho) = \oint_\Gamma \left(\{\rho \mathbf{u} X\} \cdot \mathbf{n} + \frac{\gamma_2}{2} [\![X]\!] \right) [\![r]\!] \, \mathrm{d}S - \int_\Omega (\rho \mathbf{u} X \cdot \nabla_h r) d\mathrm{V}. \tag{3.37}$$

The Lax-Friedrichs parameter γ_2 is calculated as Klein et al., 2016

$$\gamma_2 = \max \left\{ \overline{\rho^+} |\overline{\mathbf{u}^+} \cdot \mathbf{n}^+|, \overline{\rho^-} |\overline{\mathbf{u}^-} \cdot \mathbf{n}^-| \right\}. \tag{3.38}$$

The diffusion term of scalars is discretized again with a SIP formulation:

$$\mathcal{S}^D(X, r, \xi) = \int_\Omega (\xi \nabla_h X \cdot \nabla_h r) \, \mathrm{d}V - \oint_{\Gamma \setminus \Gamma_\mathrm{N} \setminus \Gamma_\mathrm{ND}} (\{\xi \nabla_h X\} \cdot \mathbf{n} [\![r]\!] + \{\xi \nabla_h r\} \cdot \mathbf{n} [\![X]\!] - \eta \xi_\mathrm{max} [\![X]\!] [\![r]\!]) \, \mathrm{d}S. \tag{3.39}$$

The transport parameter ξ is calculated as a function of temperature using Equation (2.29) and $\xi_\mathrm{max} = \max(\xi^+, \xi^-)$. The boundary condition term of the corresponding scalar equation is:

$$\mathcal{B}^3(r) = - \oint_{\Gamma_\mathrm{D} \cup \Gamma_\mathrm{ND}} \left((\rho_D \mathbf{u}_D X_D) \cdot \mathbf{n}_\Gamma + \frac{\gamma_2}{2} X_D \right) r \, \mathrm{d}S + \oint_{\Gamma_\mathrm{D} \cup \Gamma_\mathrm{ND}} \xi_D X_D (\nabla_h r \cdot \mathbf{n}_\Gamma - \eta r) \, \mathrm{d}S. \tag{3.40}$$

Here, X_D is the Dirichlet value of the scalar X on boundaries and ξ_D is the corresponding transport parameter calculated,which is calculated with Equation (2.29) using the Dirichlet values of the temperature at the boundary. Finally, the volumetric source term of the energy and mass fraction equations are defined as follows:

$$\mathcal{S}^S(r, \mathrm{Q}, \omega, c_p) = \int_\Omega \frac{\mathrm{Q}\omega}{c_p} r \, \mathrm{d}V, \tag{3.41}$$

$$\mathcal{M}^S_\alpha(s_\alpha, \omega) = \int_\Omega \nu_\alpha M_\alpha \omega s_\alpha \, \mathrm{d}V. \tag{3.42}$$

The heat release Q is calculated with Equation (2.25), the reaction rate ω is evaluated using Equation (2.24) and the mixture heat capacity with Equation (2.28).

3.1.3 Temporal discretization

Dies hier ist ein Blindtext zum Testen von Textausgaben. Wer diesen Text liest, ist selbst schuld. Der Text gibt lediglich den Grauwert der Schrift an. Ist das wirklich so? Ist es gleichgültig, ob ich schreibe: „Dies ist ein Blindtext“ oder „Huardest gefburn“? Kjift – mitnichten! Ein Blindtext bietet mir wichtige Informationen. An ihm messe ich die Lesbarkeit einer Schrift, ihre Anmutung, wie harmonisch die Figuren zueinander stehen und prüfe, wie breit oder schmal sie läuft. Ein Blindtext sollte möglichst viele verschiedene Buchstaben enthalten und in der Originalsprache gesetzt sein. Er muss keinen Sinn ergeben, sollte aber lesbar sein. Fremdsprachige Texte wie „Lorem ipsum“ dienen nicht dem eigentlichen Zweck, da sie eine falsche Anmutung vermitteln. Dies hier ist ein Blindtext zum Testen von Textausgaben. Wer diesen Text liest, ist selbst schuld. Der Text gibt lediglich den Grauwert der Schrift an. Ist

das wirklich so? Ist es gleichgültig, ob ich schreibe: „Dies ist ein Blindtext“ oder „Huardest gefburn“? Kjift – mitnichten! Ein Blindtext bietet mir wichtige Informationen. An ihm messe ich die Lesbarkeit einer Schrift, ihre Anmutung, wie harmonisch die Figuren zueinander stehen und prüfe, wie breit oder schmal sie läuft. Ein Blindtext sollte möglichst viele verschiedene Buchstaben enthalten und in der Originalsprache gesetzt sein. Er muss keinen Sinn ergeben, sollte aber lesbar sein. Fremdsprachige Texte wie „Lorem ipsum“ dienen nicht dem eigentlichen Zweck, da sie eine falsche Anmutung vermitteln. Dies hier ist ein Blindtext zum Testen von Textausgaben. Wer diesen Text liest, ist selbst schuld. Der Text gibt lediglich den Grauwert der Schrift an. Ist das wirklich so? Ist es gleichgültig, ob ich schreibe: „Dies ist ein Blindtext“ oder „Huardest gefburn“? Kjift – mitnichten! Ein Blindtext bietet mir wichtige Informationen. An ihm messe ich die Lesbarkeit einer Schrift, ihre Anmutung, wie harmonisch die Figuren zueinander stehen und prüfe, wie breit oder schmal sie läuft. Ein Blindtext sollte möglichst viele verschiedene Buchstaben enthalten und in der Originalsprache gesetzt sein. Er muss keinen Sinn ergeben, sollte aber lesbar sein. Fremdsprachige Texte wie „Lorem ipsum“ dienen nicht dem eigentlichen Zweck, da sie eine falsche Anmutung vermitteln. Dies hier ist ein Blindtext zum Testen von Textausgaben. Wer diesen Text liest, ist selbst schuld. Der Text gibt lediglich den Grauwert der Schrift an. Ist das wirklich so? Ist es gleichgültig, ob ich schreibe: „Dies ist ein Blindtext“ oder „Huardest gefburn“? Kjift – mitnichten! Ein Blindtext bietet mir wichtige Informationen. An ihm messe ich die Lesbarkeit einer Schrift, ihre Anmutung, wie harmonisch die Figuren zueinander stehen und prüfe, wie breit oder schmal sie läuft. Ein Blindtext sollte möglichst viele verschiedene Buchstaben enthalten und in der Originalsprache gesetzt sein. Er muss keinen Sinn ergeben, sollte aber lesbar sein. Fremdsprachige Texte wie „Lorem ipsum“ dienen nicht dem eigentlichen Zweck, da sie eine falsche Anmutung vermitteln. Dies hier ist ein Blindtext zum Testen von Textausgaben. Wer diesen Text liest, ist selbst schuld. Der Text gibt lediglich den Grauwert der Schrift an. Ist das wirklich so? Ist es gleichgültig, ob ich schreibe: „Dies ist ein Blindtext“ oder „Huardest gefburn“? Kjift – mitnichten! Ein Blindtext bietet mir wichtige Informationen. An ihm messe ich die Lesbarkeit einer Schrift, ihre Anmutung, wie harmonisch die Figuren zueinander stehen und prüfe, wie breit oder schmal sie läuft. Ein Blindtext sollte möglichst viele verschiedene Buchstaben enthalten und in der Originalsprache gesetzt sein. Er muss keinen Sinn ergeben, sollte aber lesbar sein. Fremdsprachige Texte wie „Lorem ipsum“ dienen nicht dem eigentlichen Zweck, da sie eine falsche Anmutung vermitteln. Dies hier ist ein Blindtext zum Testen von Textausgaben. Wer diesen Text liest, ist selbst schuld. Der Text gibt lediglich den Grauwert der Schrift an. Ist das wirklich so? Ist es gleichgültig, ob ich schreibe: „Dies ist ein Blindtext“ oder „Huardest gefburn“? Kjift – mitnichten! Ein Blindtext bietet mir wichtige Informationen. An ihm messe ich die Lesbarkeit einer Schrift, ihre Anmutung, wie harmonisch die Figuren zueinander stehen und prüfe, wie breit oder schmal sie läuft. Ein Blindtext sollte möglichst viele verschiedene Buchstaben enthalten und in der Originalsprache gesetzt sein. Er muss keinen Sinn ergeben, sollte aber lesbar sein. Fremdsprachige Texte wie „Lorem ipsum“ dienen nicht dem eigentlichen Zweck, da sie eine falsche Anmutung vermitteln. Dies hier ist ein Blindtext zum Testen von Textausgaben. Wer diesen Text liest, ist selbst schuld. Der Text gibt lediglich den Grauwert der Schrift an. Ist das wirklich so? Ist es gleichgültig, ob ich schreibe: „Dies ist ein Blindtext“ oder „Huardest gefburn“? Kjift – mitnichten! Ein Blindtext bietet mir wichtige Informationen. An ihm messe ich die Lesbarkeit einer Schrift, ihre Anmutung, wie harmonisch die Figuren zueinander stehen und prüfe, wie breit oder schmal sie läuft. Ein Blindtext sollte möglichst viele verschiedene Buchstaben enthalten und in der Originalsprache gesetzt sein. Er muss keinen Sinn ergeben, sollte aber lesbar sein. Fremdsprachige Texte wie „Lorem ipsum“ dienen

nicht dem eigentlichen Zweck, da sie eine falsche Anmutung vermitteln.

3.2 Computational methodology

The presented solver is embedded in the *BoSSS* (Bounded Support Spectral Solver) code, which is under development at the chair of fluid dynamics of the Technical University of Darmstadt, and is available under https://github.com/FDYdarmstadt/BoSSS. *BoSSS* is a general framework for the discretization of conservation laws using the DG method and uses a modal DG approach with orthonormal Legendre polynomials as basis functions. The *BoSSS* code features a variety of applications in the context of computational fluid dynamics, such as a solver for multiphase flows with a sharp interface approach, Kummer, 2017 an incompressible Immersed Boundary Method solver for particle laden flows,Krause and Kummer, 2017 a solver for viscoelastic fluid flows,Kikker et al., 2020 and a solver for compressible flows, Geisenhofer et al., 2019 among others.

The variational problem for the finite chemistry rate case described by Equations (3.26a) to (3.26d) and for the flame sheet problem, Equations (3.27a) to (3.27c), are linearised and solved using a Newton method with a Dogleg-type globalization Pawlowski et al., 2006; Pawlowski et al., 2008. The *BoSSS* framework provides an efficient algorithm for the evaluation of the Jacobian based on perturbations of the forms presented in the last section. The relatively large linear system of equations for each Newton iteration is solved by means of the in *BoSSS* integrated orthonormalization multigrid algorithm Kummer et al., 2021, which at the lowest multigrid levels makes use of the sparse direct solver PARDISO, originally developed by Schenk et al. Schenk et al., 2000; Schenk and Gärtner, 2002; Schenk and Gärtner, 2004, from the "Intel(R) Parallel Studio XE 2018 Update 3 Cluster Edition for Windows" library collection to solve the linear system.

BoSSS also features a method for solving highly nonlinear problems with a homotopy strategy. Further details on the used Newton method solver, the homotopy strategy and its implementation are given in the next sections, which are adapted from Kikker et al.Kikker et al., 2020 and are included for the sake of completeness. For information on the mentioned orthonormalization multigrid algorithm we refer the interested reader to the work of Kummer et al. Kummer et al., 2021

Calculation of the Jacobian matrix

We start by introducing a few new elements to be able to describe the implemented Newton method. The discussion for the variational problem using the mixture fraction variable (Equations (3.27a) to (3.27c)) is completely analogous, and will not be mentioned in this discussions. Find $\mathbf{U}_h \in \mathbb{V}_{\mathbf{k}}$

$$\mathcal{N}(\mathbf{U}_h, \mathbf{V}_h) = 0 \quad \forall\, \mathbf{V}_h \in \mathbb{V}_{\mathbf{k}}, \tag{3.43}$$

for $\mathbf{U}_h = (p_h, \mathbf{u}_h, T_h, \mathbf{Y}'_h)$ and $\mathbf{V}_h = (q_h, \mathbf{v}_h, r_h, \mathbf{s}_h)$. We assume a basis $\underline{\mathbf{\Phi}} = (\mathbf{\Phi}_1, \ldots, \mathbf{\Phi}_L)$ of $\mathbb{V}_{\mathbf{k}}$, written as a row vector, with $L \coloneqq \dim(\mathbb{V}_{\mathbf{k}})$. Then $\mathbf{U}_h$ can be represented as $\mathbf{U}_h = \underline{\mathbf{\Phi}} \cdot \mathbf{U}$. The nonlinear problem (3.43) can then be written as

$$\mathcal{A}(\mathbf{U}) = 0, \tag{3.44}$$

with the nonlinear function $\mathbb{R}^L \ni \mathbf{U} \mapsto \mathcal{A}(\mathbf{U}) \in \mathbb{R}^L$. The i-th component of $\mathcal{A}(\mathbf{U})$, can be defined by $\mathcal{N}(-,-)$ through the relation $[\mathcal{A}(\mathbf{U})]_i = \mathcal{N}(\underline{\mathbf{\Phi}} \cdot \mathbf{U}, \mathbf{\Phi}_i)$.

The formulation of the Newton method requires the Jacobian matrix $\partial\mathcal{A}$ of $\mathcal{A}$, defined as

$$\partial\mathcal{A}_{ij}(\mathbf{U}) \coloneqq \frac{\partial\mathcal{A}_i}{\partial U_j}(\mathbf{U}). \tag{3.45}$$

Its computation is quite straightforward, but lengthy. The *BoSSS* code is capable of evaluating the Jacobian matrix automatically from the expressions given in Section 3.1.1. We note that one could write $\mathcal{A}(\mathbf{U})$ as

$$[\mathcal{A}(\mathbf{U})]_i = \mathcal{N}(\mathbf{U}_h, \mathbf{\Phi}_i) = \int_{\Omega_h} N_1(\mathbf{x}, \mathbf{U}_h, \nabla\mathbf{U}_h)\cdot\mathbf{\Phi}_i + N_2(\mathbf{x}, \mathbf{U}_h, \nabla\mathbf{U}_h)\cdot\nabla\mathbf{\Phi}_i \mathrm{dV} + \oint_\Gamma \ldots \mathrm{dS}. \tag{3.46}$$

The edge integral, which is left out in Equation (3.46), can be written in analogous fashion as the volume integral, i.e. as a sum over four nonlinear functions, multiplied by $\mathbf{\Phi}_i^+$, $\mathbf{\Phi}_i^-$, $\nabla\mathbf{\Phi}_i^+$ and $\nabla\mathbf{\Phi}_i^-$, respectively. These functions themselves may depend on $\mathbf{x}$, $\mathbf{U}_h^+$, $\mathbf{U}_h^-$, $\nabla\mathbf{U}_h^+$ and $\nabla\mathbf{U}_h^-$. For sake of compactness, this part is skipped. Realizing that $\frac{\partial\mathbf{U}_h}{\partial\mathbf{U}_j} = \mathbf{\Phi}_j$ and by application of the chain rule, one derives

$$\partial\mathcal{A}_{ij}(\mathbf{U}) = \int_{\Omega_h} (\partial_{\mathbf{U}_h} N_1(\mathbf{x}, \mathbf{U}_h, \nabla\mathbf{U}_h)\mathbf{\Phi}_j + \partial_{\nabla\mathbf{U}_h} N_1(\mathbf{x}, \mathbf{U}_h, \nabla\mathbf{U}_h)\nabla\mathbf{\Phi}_j)\cdot\mathbf{\Phi}_i + \ldots \mathrm{dV} + \oint_\Gamma \ldots \mathrm{dS}. \tag{3.47}$$

All skipped terms in Equation (3.47) can be derived in an analogous fashion as the contributions for N_1. In the *BoSSS* code, derivatives $\partial_{\mathbf{U}_h} N_1(\ldots)$ and $\partial_{\nabla\mathbf{U}_h} N_1(\ldots)$ are approximated by a finite difference, using a perturbation by $\sqrt{\texttt{eps}}$ in the respective argument, where $\texttt{eps} = 2.22044604925031 \cdot 10^{-16}$ is the floating point accuracy for double precision.

The notation introduced here allows us to describe the Newton-Dogleg method used in this work. We note however that this globalization strategy is still not sufficient to ensure convergence for some of the test cases presented, namely for high Rayleigh numbers for the differentially heated cavity problem. For those cases we use a homotopy strategy, where we start with a low homotopy-parameter, a parameter for which the solution of the problem is not hard to find, which is gradually and carefully increased until convergence for the desired value of the homotopy-parameter is reached (cf. Section 3.2.4).

3.2.1 Dogleg Method

We consider a linearization of Equation (3.44) around $\mathbf{U}_n$,

$$\mathcal{A}(\mathbf{U}_n) + \partial\mathcal{A}(\mathbf{U}_n)\underbrace{(\mathbf{U}_{n+1} - \mathbf{U}_n)}_{=:\mathbf{s}'_n} = 0. \tag{3.48}$$

By repeatedly solving this system one obtains a standard Newton scheme for Equation (3.44), yielding a sequence of approximate solutions $\mathbf{U}_0, \mathbf{U}_1, \mathbf{U}_2, \ldots$ obtained from an initial guess $\mathbf{U}_0$ through the iteration scheme $\mathbf{U}_{n+1} = \mathbf{U}_n + \mathbf{s}'_n$. In the classical un-damped Newton method, the correction step $\mathbf{s}'_n$ is set to be the whole Newton-step, i.e $\mathbf{s}'_n = \mathbf{s}_n$ with

$$\mathbf{s}_n \coloneqq -\partial\mathcal{A}(\mathbf{U}_n)^{-1}\mathcal{A}(\mathbf{U}_n), \tag{3.49}$$

which is computed using a direct solver. Unfortunately, convergence of the Newton method for any starting value $\mathbf{U}_0$ is not guaranteed. In order to increase robustness when the distance between $\mathbf{U}_0$ and the exact solution $\mathbf{U}$ is large, we employ a globalization approach, presented by

Pawlowski et al. Pawlowski et al., 2006; Pawlowski et al., 2008, known as the Dogleg-method, or Newton-Dogleg method. Here, we intend to give only the central ideas of method and refer to the original works for further details. Obviously, the exact solution of Equation (3.44) is also a minimum of the functional

$$f(\mathbf{U}) \coloneqq \frac{1}{2} \|\mathcal{A}(\mathbf{U})\|_2^2 . \tag{3.50}$$

One observes that $\nabla f(\mathbf{U}) = \partial\mathcal{A}(\mathbf{U})^T \mathcal{A}(\mathbf{U})$. For $\mathbf{U}_n$, the approximate Cauchy point with respect to the 2-norm, is defined as the minimizer $\mathbf{g}_n$ of $\|\mathcal{A}(\mathbf{U}_n) + \partial\mathcal{A}(\mathbf{U}_n)\mathbf{g}_n\|_2$ in the direction of steepest decent, i.e. $\mathbf{g}_n = \lambda \nabla f(\mathbf{U}_n)$, $\lambda \in \mathbb{R}$. Substituting $\mathbf{w} \coloneqq -\partial\mathcal{A}(\mathbf{U}_n)\nabla f(\mathbf{U}_n)$, $\mathbf{g}_n$ is given by

$$\mathbf{g}_n = \frac{\mathcal{A}(\mathbf{U}_n) \cdot \mathbf{w}}{\mathbf{w} \cdot \mathbf{w}} \nabla f(\mathbf{U}_n). \tag{3.51}$$

For the Newton-Dogleg method, the correction step $\mathbf{s}'_n$ is chosen along the so-called Dogleg curve, which is the piece-wise linear curve from the origin to $\mathbf{g}_n$ and further to $\mathbf{s}_n$. The selection of $\mathbf{s}'_n$ on this curve is determined by the trust-region diameter $\delta > 0$:

- If $\|\mathbf{s}_n\|_2 \leq \delta$, $\mathbf{s}'_n = \mathbf{s}_n$.
- If $\|\mathbf{g}_n\|_2 \leq \delta$ and $\|\mathbf{s}_n\|_2 > \delta$, $\mathbf{s}'_n$ is chosen on the linear interpolation from $\mathbf{g}_n$ to $\mathbf{s}_n$ so that $\|\mathbf{s}'_n\|_2 = \delta$: For the ansatz $\mathbf{s}'_n = \tau\mathbf{s}_n + (1-\tau)\mathbf{g}_n$, the interpolation factor τ is given as $\tau = (a^2 - c + \sqrt{(a^2+b^2-2c)\delta^2 - a^2b^2 + c^2})/(a^2+b^2-2c)$ with $a = \|\mathbf{g}_n\|_2$, $b = \|\mathbf{s}_n\|_2$ and $c = \mathbf{g}_n \cdot \mathbf{s}_n$.
- If $\|\mathbf{g}_n\|_2 > \delta$, $\mathbf{g}_n = (\delta / \|\mathbf{g}_n\|_2)\mathbf{g}_n$.

The choice and adaptation of the trust region diameter δ throughout the Newton-Dogleg procedure follows a sophisticated heuristic, mainly based on comparing the actual residual reduction $\text{ared}_n \coloneqq \|\mathcal{A}(\mathbf{U}_n)\|_2 - \|\mathcal{A}(\mathbf{U}_n + \mathbf{s}'_n)\|_2$ with the predicted residual reduction $\text{pred}_n \coloneqq \|\mathcal{A}(\mathbf{U}_n)\|_2 - \|\mathcal{A}(\mathbf{U}_n) + \partial\mathcal{A}(\mathbf{U}_n)\mathbf{s}'_n\|_2$; For the direct solver used in this work pred_n simplifies to $\text{pred}_n \coloneqq \|\mathcal{A}(\mathbf{U}_n)\|_2$. We replicate the algorithm here, for the sake of completeness:

(1) Set $n = 0$, $\delta_n = \min(10^{10}, \max(2 \cdot 10^{-6}, \|\mathbf{s}_0\|_2))$.

(2) Compute the Newton step $\mathbf{s}_n$ and the Cauchy point $\mathbf{g}_n$ and find $\mathbf{s}'_n$ on the Dogleg curve with respect to the recent δ_n.

(3) While $\text{ared}_n \leq \text{pred}_n$ do: Update trust region diameter $\delta_n \leftarrow 0.5\ \delta_n$ and re-compute $\mathbf{s}'_n$. If $\delta_n < 10^{-6}$ terminate abnormally and mark the computation as failed.

(4) If the convergence criterion (see below) is fulfilled, terminate and mark the computation as success.

(5) Perform a final update of the trust region: Set

$$\delta_{n+1} = \begin{cases} \max(10^{-6}, \|\mathbf{s}_n\|_2) & \text{if } \text{ared}_n/\text{pred}_n < 0.1 \text{ and } \|\mathbf{s}_n\|_2 \delta_n \\ \max(10^{-6}, 0.25 \cdot \delta_n) & \text{else, if } \text{ared}_n/\text{pred}_n < 0.1 \\ \min(10^{10}, 4 \cdot \delta_n) & \text{else, if } \text{ared}_n/\text{pred}_n > 0.75 \\ \delta_n & \text{otherwise} \end{cases}$$

Set $\mathbf{U}_{n+1} = \mathbf{U}_n + \mathbf{s}'_n$, update $n \leftarrow n+1$ and return to step (2).

All constants used in the algorithm above have been taken from the work of Pawlowski et al. Pawlowski et al., 2006 For a detailed description of the underlying ideas we also refer to these works, which in turn are based on algorithms from Dennis and Schnabel's textbook. Dennis and Schnabel, 1996

3.2.2 Termination criterion

A simple approach to determine that a Newton-Dogleg loop can be terminated is to check whether the residual norm has fallen below a certain threshold, i.e. $\|\mathcal{A}(U_n)\| \leq \text{tol}$. A universal choice for the tolerance is indeed difficult, especially for investigations of convergence properties (cf. **??** and **??**). If it is chosen too low, the algorithm may never terminate, because of dominating numerical round-off errors. On the other hand, if it is chosen too high, the error of the premature termination may dominate the error of the spatial discretization and one cannot take the full advantage of the high-order method. Therefore the goal is to continue the Newton-Dogleg method until the lowest possible limit dictated by floating point accuracy is reached. To identify the limit in a robust way, we first define the residual-norm skyline as

$$\text{sr}_n := \min_{j \leq n} \|\mathcal{A}(\mathbf{U}_j)\| \tag{3.52}$$

and, for $n \geq 2$, the averaged reduction factor

$$\text{arf}_n := \frac{1}{2}\left(\frac{\text{sr}_{n-2}}{\max\{\text{sr}_{n-1}, 10^{-100}\}} + \frac{\text{sr}_{n-1}}{\max\{\text{sr}_n, 10^{-100}\}}\right). \tag{3.53}$$

The Newton-Dogleg method is terminated if

$$n \geq 2 \text{ and } \text{sr}_n \leq 10^{-5} + 10^{-5}\|\mathbf{U}_n\|_2 \text{ and } \text{arf}_n < 1.5. \tag{3.54}$$

For the computations in this work, this choice guarantees that the nonlinear system is solved as accurately as possible. It secures that the numerical error is dominated by the error of the spatial or temporal discretization and not by the termination criterion of the Newton-Dogleg method. The skyline approach ensures robustness against oscillations close to the lower limit.

3.2.3 Solver safeguard

3.2.4 Homotopy method

Although the Newton-Dogleg method works well for a variety of cases, we experienced convergence problems for some of the test cases presented in next section. In particular, for the differentially heated cavity test case, the method was not successful on finding a convergent solution for a Rayleigh number $Ra \geq 10^5$ within 60 Newton iterations. In such cases we used a homotopy strategy, which is loosely based on ideas from the textbook of Deuflhard,Deuflhard, 2011 Chapter 5.

We start by identifying a parameter that makes the solution of the nonlinear problem difficult to solve. In the following we will refer to this variable as the homotopy parameter. The main idea of the homotopy strategy consists of solving a series of simpler problems, starting with a parameter where the problem is easy to solve, and carefully increasing it until the desired value is reached. Let Hp denote the value of the homotopy parameter for which a solution is being sought. Let

$$\mathcal{A}_{\mathrm{hp}^*}(\mathbf{U}) = 0 \tag{3.55}$$

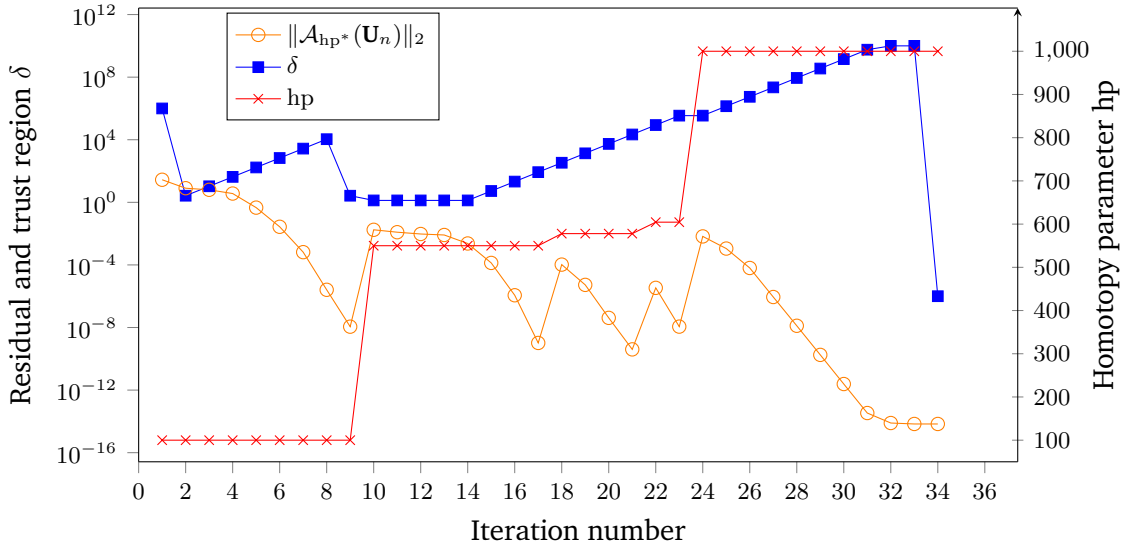

Figure 3.1: Behaviour of the homotopy method for the differentially heated cavity test case. The homotopy parameter hp in this case is the Reynolds number.

be the discretized system for a certain intermediate homotopy-parameter hp^*, between 0 and the 'target' homotopy-parameter Hp, i.e. $0 \leq \mathrm{hp}^* \leq \mathrm{Hp}$. Furthermore, let $\mathbf{U}_{\mathrm{hp},\epsilon}$ be an approximate solution to the problem (3.55) with $\mathrm{hp}^* = \mathrm{hp}$, up to a tolerance ϵ, i.e.

$$\|\mathcal{A}_{\mathrm{hp}}(\mathbf{U}_{\mathrm{hp},\epsilon})\|_2 \leq \epsilon. \tag{3.56}$$

For the sake of clarity when discussing the algorithm which follows below, we distinguish between the intermediate homotopy-parameter hp for which we assume to already have found an acceptable solution and the next homotopy-parameter hp^* that we are currently trying to find a solution for. For any $\mathrm{hp}^* > \mathrm{hp}$ we set $\epsilon = 10^{-5}\,\|\mathcal{A}_{\mathrm{hp}*}(\mathbf{U}_{\mathrm{hp},\epsilon})\|_2$, i.e. we aim for a residual norm reduction of at least five orders of magnitude with respect to the initial residual norm. If $\mathrm{hp}^* = \mathrm{Hp}$, the termination criterion presented in section 3.2.2 is applied. An approximate solution for the target homotopy-parameter is found by the following recipe:

(1) Set $\mathrm{hp} = 0$, i.e. start by obtaining an (approximate) solution $\mathbf{U}_{0,\epsilon}$.

(2) Search for a an increased homotopy-parameter hp^*: Find the minimal $i \geq 0$ so that for $\mathrm{hp}^* = \frac{1}{2^i}(\mathrm{Hp} - \mathrm{hp}) + \mathrm{hp}$ one has $\left\|\mathcal{A}_{\mathrm{hp}^*}(\mathbf{U}_{\mathrm{hp},\epsilon})\right\|_2 \leq \delta_{\max}\,\|\mathcal{A}_{\mathrm{hp}}(\mathbf{U}_{\mathrm{hp},\epsilon})\|_2$ Here, $\delta_{\max}$ is the maximal allowed increase of the residual for an increased homotopy-parameter hp^*; $\delta_{\max}$ is adapted in the following steps, as an initial guess we use $\delta_{\max} = 10^6$.

(3) Use the Newton-Dogleg method to compute an approximate solution to the problem (3.55), for the homotopy-parameter hp^*, using the solution $\mathbf{U}_{\mathrm{hp},\epsilon}$ as an initial guess.

- If the Newton-Dogleg method did not converge successfully within ten steps, the homotopy-parameter increase from hp to hp^* was probably too large. Set $\delta_{\max} \leftarrow 0.2\delta_{\max}$ and go to step (2).
- If the Newton-Dogleg method reached its convergence criterion and if the target homotopy-parameter is reached, i.e. $\mathrm{hp}^* = \mathrm{Hp}$, the algorithm has successfully found an approximate solution for $\mathcal{A}_{\mathrm{Hp}}(\mathbf{U}) = 0$ and can terminate.

– Otherwise, if the Newton-Dogleg method converged successfully, but is below the target homotopy-parameter: Accept the solution and set $\mathrm{hp} \leftarrow \mathrm{hp}^*$. If the Newton-Dogleg method took less than three iterations to reach the convergence criterion, set $\delta_{\max} \leftarrow 8\delta_{\max}$. Return to step (2).

An exemplary run of the method is shown in Figure 3.1. The homotopy parameter hp in this particular case is the Reynolds number. The homotopy-parameter hp was increased for iterations 10, 18, 22 and 24, causing an increase of the residuals $\|\mathcal{A}_{\mathrm{hp}^*}(\mathbf{U}_n)\|_2$, leading to a convergent solution after 34 Newton iterations. The presented algorithm offers a robust method for finding steady-state solutions of highly nonlinear systems.

3.2.5 Initialization of combustion applications

Cases involving combustion are initialized with the solution of the flame sheet problem, Equations (3.27a) to (3.27c). This idea has been already employed in various works. Smooke et al., 1986; Smooke and Giovangigli, 1992 The reason for the use of this pre-step is twofold:

- Solving **????** and Equations (2.22c) and (2.22d) using a Newton-type method requires adequate starting estimates in order to converge. Using the flame sheet solution as initial estimate improves the convergence properties of the method.
- The system of **????** and Equations (2.22c) and (2.22d) possesses multiple solutions. One is the pure mixing (frozen) solution, where no chemical reaction has taken place, and the other one is the ignited solution, where the flame is present. Using the flame sheet solution as initial estimate ensures that the path taken by Newton's algorithm will tend towards the ignited solution.

We remark at this point that although for the solution of the flame sheet system the mixture heat capacity has been assumed to be constant, it remains an adequate estimate for the finite reaction-rate problem, where the heat capacity is a function of temperature and local concentration. In a similar fashion, the assumption of unity Lewis number in the flame sheet system delivers a solution that slightly deviates from the solution of the finite chemistry rate problem with non-unity Lewis numbers. Nevertheless, this small deviation does not preclude the use of the flame sheet solution as an adequate initial estimate for Newton's method.

Regarding the solution of the flame sheet problem (cf. Section 2.2), it should be noted that the sharp change in the primitive variables around $z = z_{st}$ could be problematic. In particular, the non-smoothness of the derived variables could lead to Gibbs phenomenon-type problems. This inconvenient can be remedied by using a regularized form of the equations. We define the smoothing function $\mathcal{H}$

$$\mathcal{H}(z) \approx \frac{1}{2}(1 + \tanh(\frac{z - z_{st}}{\sigma})), \tag{3.57}$$

The parameter σ dictates the sharpness of the transition at $z = z_{st}$. In Figure 3.2 the effect of the smoothing factor σ on calculations of a flame in a counter-flow configuration are shown. It can be clearly observed how for increasing σ the solution becomes smoother. Using Equation (3.57) the temperature and mass fraction fields can be written as

$$T(z) = zT_F^0 + (1 - z)T_O^0 + \frac{QY_F^0}{c_p} z_{st} \frac{1 - z}{1 - z_{st}} \mathcal{H}(z) + \frac{QY_F^0}{c_p} z \left(1 - \mathcal{H}(z)\right), \tag{3.58}$$

$$Y_F(z) = Y_F^0 \frac{z - z_{st}}{1 - z_{st}} \mathcal{H}(z), \tag{3.59}$$

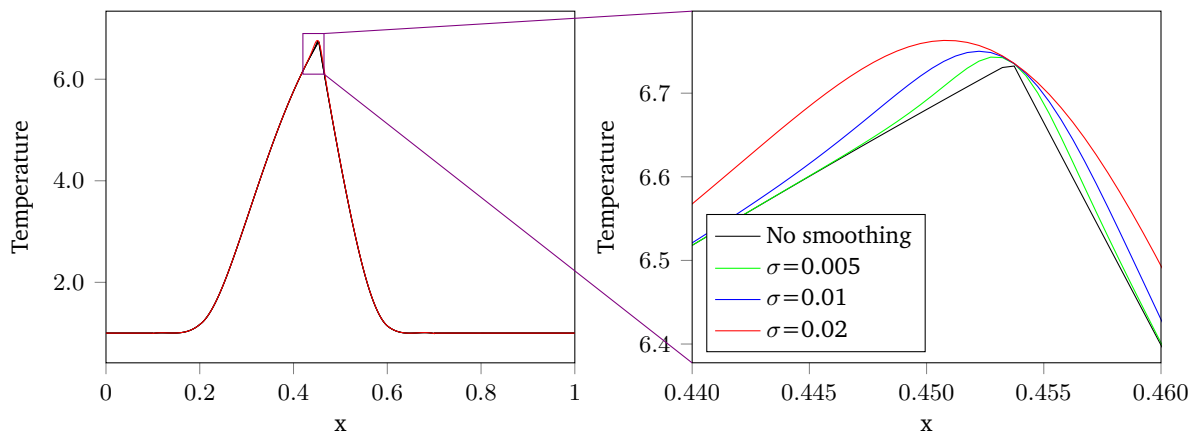

Figure 3.2: Temperature profile calculated in the center-line of a counter-flow flame configuration for different smoothing parameters σ.

$$Y_O(z) = Y_O^0 \frac{z_{st} - z}{z_{st}}(1 - \mathcal{H}(z)), \tag{3.60}$$

$$Y_P(z) = Y_O^0 \frac{M_P \nu_P}{M_O \nu_O}(1 - z)\mathcal{H}(z) + Y_F^0 \frac{M_P \nu_P}{M_F \nu_F} z(1 - \mathcal{H}(z)). \tag{3.61}$$

$$Y_N(z) = (1 - Y_F^0)z + (1 - Y_O^0)(1 - z). \tag{3.62}$$

The use of this regularized form of the equations results in practice on a spreading of the flame front, which eases the numerical calculation (Braack et al., 1997).

We note at this point that Equation (2.20) yields unphysical values of $\hat{Q}$ for large values of ϕ. This problem can be avoided by setting an upper boundary value for ϕ in Equation (2.20) (we use $\phi = 1.2$). In practice however, this should not have a significant effect, because the unphysical values of $\hat{Q}$ appear at zones where the reaction rate $\hat{\omega}$ is very close to zero, making the factor $\hat{Q}\hat{\omega}$ in the temperature equation negligible. Nevertheless, setting an upper bound for ϕ is helpful to avoid possible numerical instabilities.

Adaptive Mesh Refinement

4 Results

In the following sections a comprehensive validation of the solver presented previously using a variety of benchmark cases will be presented. The chosen test cases will be presented incrementally in complexity. In Section 4.1 the applicability of the solver for isothermal single-component systems is analyzed. Later in Section 4.2 several single-component non-isothermal configurations are studied. Finally in **??** test-cases for multi-component non-isothermal systems are presented.

All calculations shown here where performed on AMD EPYC 7543 32-Core Processor, DDR4 Si no es stated otherwise, all calculations use the termination criterion presented in Section 3.2.2

4.1 Single-component isothermal cases

The solver presented in the previous sections is initially validated for single-component isothermal cases. In these cases only the continuity and momentum equations are solved. The energy and species concentration equations are replaced by the condition $T = 1.0$ and $Y_0 = 1.0$ in the complete domain. This means that the physical properties of the flow (density and viscosity) are constants and the flow is completely incompressible.

4.1.1 Lid-driven cavity flow

The lid-driven cavity flow is a test problem classically used for the validation of Navier-Stokes solvers. The system configuration is shown in Figure 4.1. It consists simply of a two-dimensional square cavity enclosed by walls whose upper boundary moves at constant velocity, causing the fluid to move. This provides a simple test-case which can be used for the validation of incompressible Navier-Stokes solvers. Benchmarks results can be found widely in the available

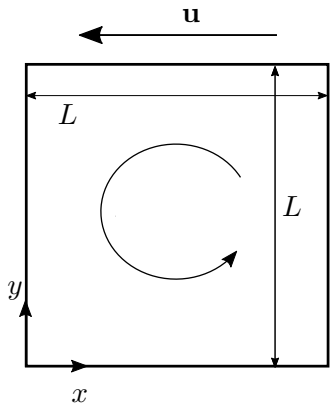

Figure 4.1: Schematic representation of the Lid-Driven cavity flow.

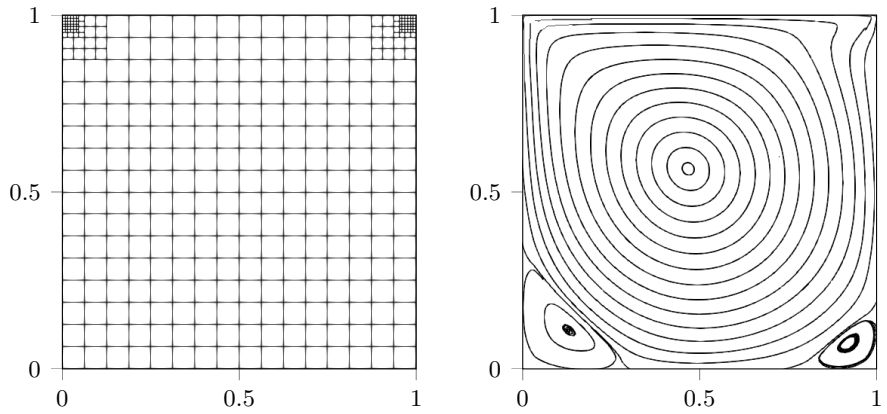

Figure 4.2: Used mesh and streamlines obtained for the lid-driven cavity flow with Re $= 1000$

literature for different Reynolds numbers. We compare in this section our results with the ones published by Botella and Peyret, 1998 and focus in the case where Re $= 1000$.

The problem is defined in the domain $\Omega = [0, 1] \times [0, 1]$. The system is solved for the velocity vector $\mathbf{u} = (u, v)$ and the pressure p. All boundary conditions are of the Dirichlet type, particularly with $\mathbf{u} = (-1, 0)$ for the boundary at $y = 1$, and $\mathbf{u} = (0, 0)$ for all other sides. The gravity vector is set to $\mathbf{g} = (0, 0)$.

In Figure 4.2 the used mesh is presented, which corresponds to a Cartesian mesh with extra refinement on both upper corners. This was done to be able to better represent the complex effects that take place there. The streamlines plot presented in Figure 4.2 show the different vortex structures typical to this kind of systems. Additional to the main vortex, smaller structures appear in the corners of the cavity.

In Figure 4.3 a comparison of the calculated velocity and the velocities provided by the benchmark are shown. For the calculations presented here, the polynomial degree is set to $k = 4$ and $k' = 3$. A regular cartesian mesh with 16×16 elements with extra refinement in the corners is used. Clearly a very good agreement is obtained, even by using a relatively coarse mesh (the benchmark result uses a grid with 160×160 elements).

A more rigorous comparison of results is presented in Table 4.1, where the extreme values of the velocity components calculated through the centerline of the cavity are compared with the results presented by Botella and Peyret, 1998. We use for this comparison different mesh resolutions. It can be clearly seen how for the 256×256 mesh the results obtained with our solver are extremely close to the reference, seeing a difference only at the fifth digit after the decimal point for the velocity components, and no difference for the spatial coordinates where the extrema are. It can also be appreciated how the results obtained with the coarser meshes are still very close to those of the reference. It is worth mentioning this comparison here could be considered unfair, since the simulations were performed with polynomial degrees of degree 4 for the velocity and three for the pressure, while the calculations of the reference use This point will be further discussed in later sections.

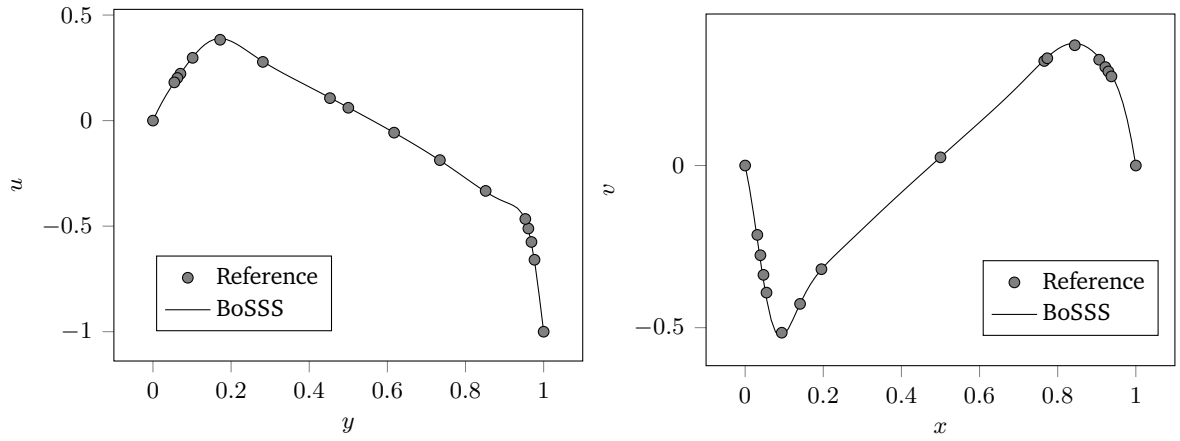

Figure 4.3: Calculated velocities along the centerlines of the cavity and reference values. Left plot shows the x-velocity for $x = 0.5$. Right plot shows the y-velocity for $y = 0.5$

Mesh	$u_{\max}$	$y_{\max}$	$v_{\max}$	$x_{\max}$	$v_{\min}$	$x_{\min}$
16×16	0.3852327	0.1820	0.3737295	0.8221	-0.5056627	0.0941
32×32	0.3872588	0.1821	0.3760675	0.8227	-0.5080496	0.0943
64×64	0.3897104	0.1748	0.3774796	0.8408	-0.5248360	0.0937
128×128	0.3886452	0.1720	0.3770127	0.8422	-0.5271487	0.0907
256×256	0.3885661	0.1717	0.3769403	0.8422	-0.5270653	0.0907
Reference	0.3885698	0.1717	0.3769447	0.8422	-0.5270771	0.0908

Table 4.1: Extrema of velocity components through the centerlines of the cavity for Re $= 1000$. Reference values obtainder from Botella and Peyret, 1998

4.1.2 Backward-facing step

The backward-facing step problem is another classical configuration widely used for validation of incompressible CFD codes. It has been widely studied theoretically, experimentally and numerically by many authors in the last decades (see for example Armaly et al., 1983; Barkley et al., 2000; Biswas et al., 2004). In Figure 4.4 a schematic representation of the problem is shown. It consists of a flow (usually considered fully developed) that is subjected to a sudden change in geometry, which causes separation and reattachment phenomena. For these reasons, this case can be considered more challenging than the one presented in the previous section, since special care of the used geometry has to be taken in order to capture accurately all complex phenomena taking place.

Although The backward-facing step problem is known to be inherently three-dimensional, it has been shown that it can be studied as a two-dimensional configuration along the symmetry plane for moderate Reynolds numbers (Barkley et al., 2000; Biswas et al., 2004). For the range of Reynolds numbers used in our calculations the two-dimensional assumption is justified. The origin of the coordinate system is set at the bottom part of the step. The step height S and channel height h characterize the system. The results on the literature are often reported as a function of the expansion ratio, defined as ER $= (\mathrm{h} + \mathrm{S})/\mathrm{h}$. We conduct a series of simulations with the objective of reproducing the results reported in Biswas et al., 2004, where the backward-facing step was calculated for Reynolds numbers up to 400 and for a expansion ratio of 1.9423. The Reynolds number for the backward-facing step configuration is defined

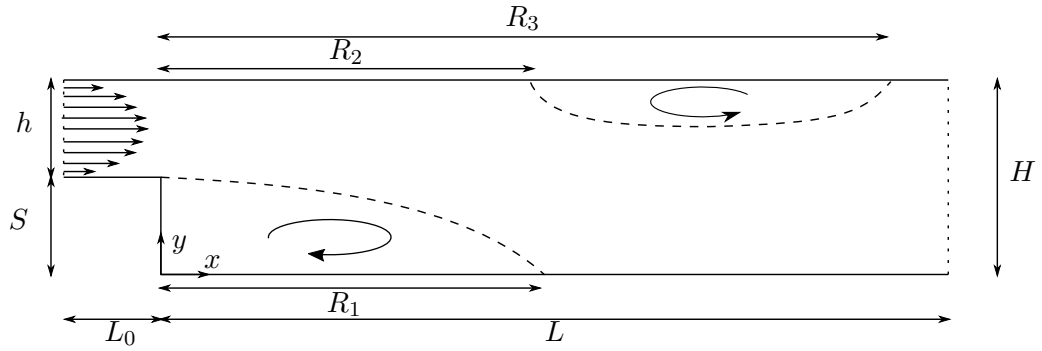

Figure 4.4: Schematic representation of the backward-facing step. Both primary and secondary vortices are shown. Sketch is not to scale.

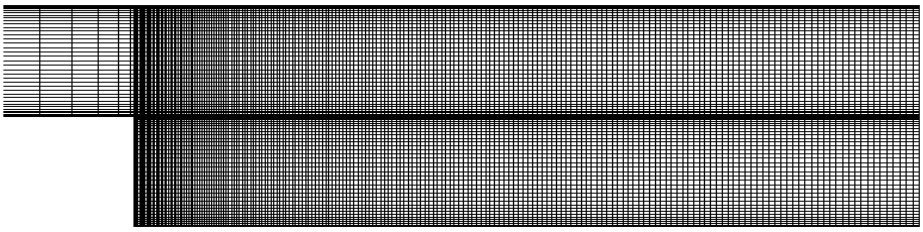

Figure 4.5: Structured mesh used in all calculations.

in the literature in many forms. We adopt here the definition based on the step height S and mean inlet velocity U_{mean} as reference values, resulting in

$$\text{Re} = \frac{\text{S}U_{\text{mean}}}{\nu} \tag{4.1}$$

The system is isothermal and the fluid is assumed to be air. The inlet profile is parabolic and is given by

$$u(y) = -6U_{\text{mean}}\frac{(y-S)(y-(h+S))}{h^2} \tag{4.2}$$

In order to minimize the effects of the outlet boundary condition in the system, the length L of the domain was set to $L = 70\text{S}$. Additionally $L_0 = \text{S}$. For all calculations in this section an structured grid with 88400 elements is used. To better resolve the complex structures that occur in this configuration, smaller elements are used in the vicinity of the step, as seen in figure Figure 4.5.

The backward-facing step configuration exhibits varying behaviour as the number of Reynolds changes. At small Reynolds number, a single vortex, usually called the primary vortex, appears in the vicinity of the step. In addition, as the Reynolds number increases, a second vortex eventually appears on the top wall, as is shown schematically in Figure 4.4. The detachment and reattachment lengths of the vortices are values usually reported in the literature. It is possible to determine the position of deattachment by finding the point along the wall where the velocity gradient acquires a value equal to zero. Figure 4.6 shows the deattachment and reattachment lenghts of the primary and secondary vortices obtained with our code for different Reynolds numbers, which are also compared with the results presented in the reference Biswas et al., 2004. It can be observed how the results for the deattachment lengths of the primary

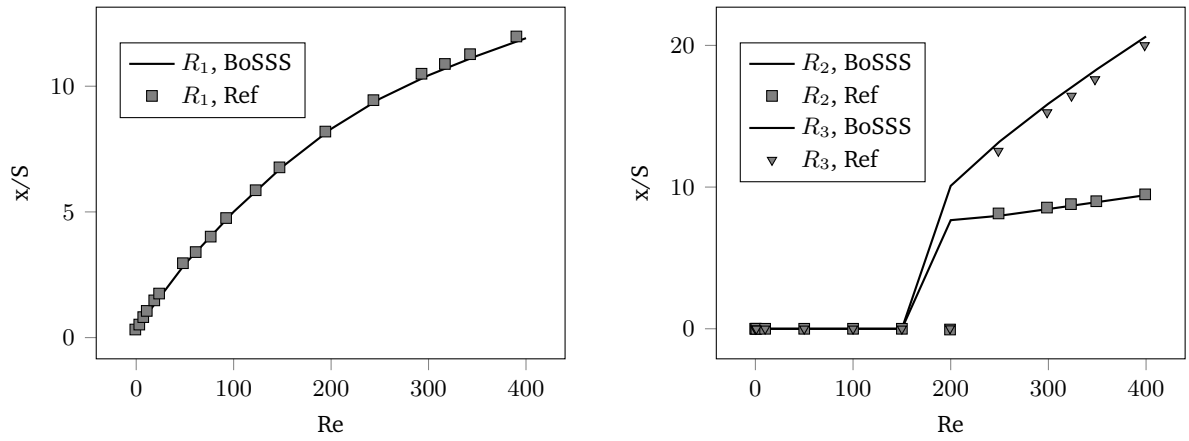

Figure 4.6: Detachment and reattachment lengths of the primary (left figure) and secondary (right figure) recirculation zones after the backward-facing step. Solid lines correspond to the results obtained with BoSSS and the marks to the reference solution (Biswas et al., 2004).

vortex present very good agreement with those of the reference. In the case of the secondary vortex it is possible to see a very minimal deviation for the reattachment lenghts. It is interesting to note that despite the fact that the reference does not report the existence of a secondary vortex for Re $= 200$, with our code it was possible to observe it. The results allow us to conclude that it is possible to study flows with complex behavior for high Reynolds numbers, at least in the isothermal case. In the next section we will discuss what happens for the non-isothermal case.

It is worth mentioning that the evaluation of the numerical accuracy of the solver using both incompressible test cases presented in this section is problematic due to singularities appearing. Nevertheless, the good agreement of our results with the benchmark let us conclude that the solver is able of simulating incompressible flows.

4.2 Single-component non-isothermal cases

Here the equations for continuity, momentum and energy are solved (Equations (2.22a) to (2.22c)). All systems are asumed to be single-component, thus $N = 1$ and $Y_0 = 1.0$. In section Section 4.2.2 a Couette flow presenting a temperature gradient in the vertical direction is studied.

In **??** a heated square cavity configuration is studied in order to asses the capability of the solver for variable density flows in closed systems. Later in in **??** and **??** two different configurations for reactive flows are presented.

4.2.1 Heated backward-facing step

As an extension to the previous case, we seek to recreate the results presented in Xie and Xi, 2016, where the same backward-facing step configuration as presented above is studied, but with the particularity that in this case the bottom wall is heated to a constant temperature, thus featuring a non-isothermal system. The fluid entering the system has a temperature equal to $T_0 = 10C$ and the bottom wall is set to a constant temperature of $T_1 = 40C$. In Xie and Xi, 2016 results are reported for the local Nusselt numbers and local friction coefficients f_d

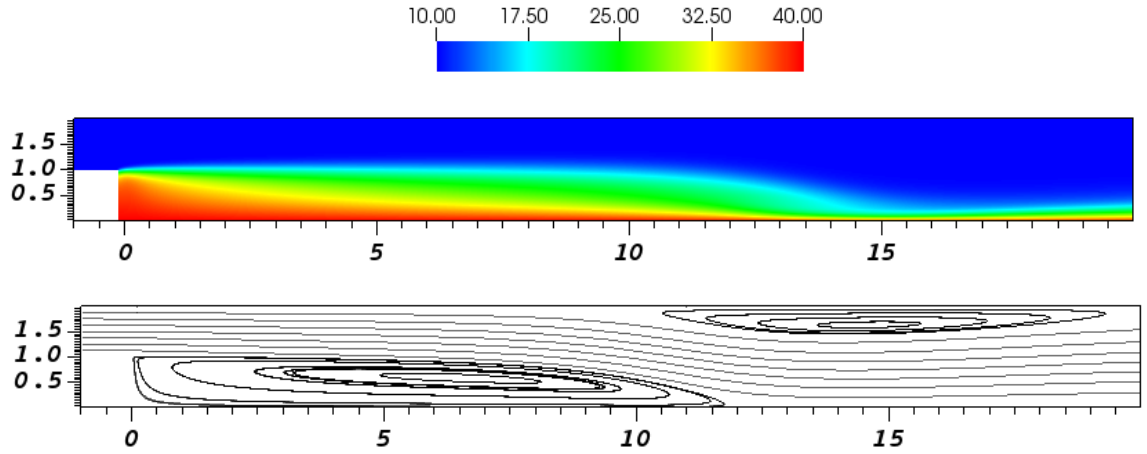

Figure 4.7: Temperature profile (top) and streamlines (bottom) corresponding to the backward-facing Step configuration for Re $= 400$ and an expansion ratio of two.

along the bottom wall for different expansion ratios and Reynolds numbers. The local Nusselt number is defined as

$$\mathrm{Nu} = \frac{S}{T_0 - T_1} \nabla T \cdot \mathbf{n} \tag{4.3}$$

On the other hand, and by recognizing that the wall shear stress along the bottom wall $\tau_\mathrm{w} = -\mu \nabla u \cdot \mathbf{n}$, the local friction factor can be written as

$$f_d = \frac{8\nu}{(U_\mathrm{mean})^2} \nabla u \cdot \mathbf{n} \tag{4.4}$$

A series of simulations for varying Reynolds numbers and expansion ratios were conducted. In Figure 4.7 the temperature field and streamlines corresponding to a calculation with Re $= 700$ is shown. Here the apparition of the secondary vortex is appreciated. We point out here that the results obtained by us are substantially different from those reported in Xie and Xi, 2016, and will not be shown here. Nevertheless, in the work of Hennink, 2022 the same is also pointed out, saying that with his method it was not possible to reproduce the results presented by Xie and Xi, 2016. Comparing our results with those of Hennink we can see that the same results are obtained, as demonstrated in Figure 4.8.

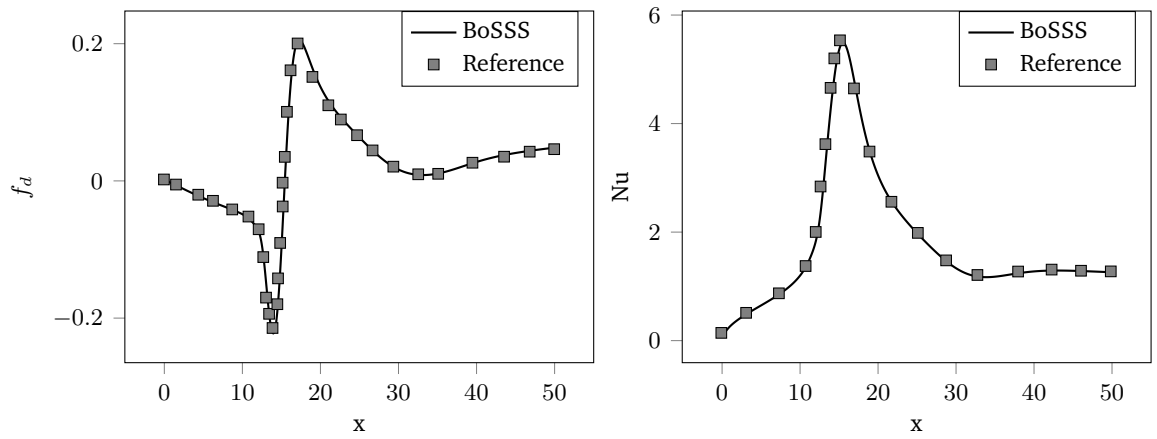

Figure 4.8: Local friction factor and local Nusselt number along the bottom wall for Re $= 700$ and an expansion ratio of two. The solid lines corresponds to our solution and the marks to the reference Hennink, 2022

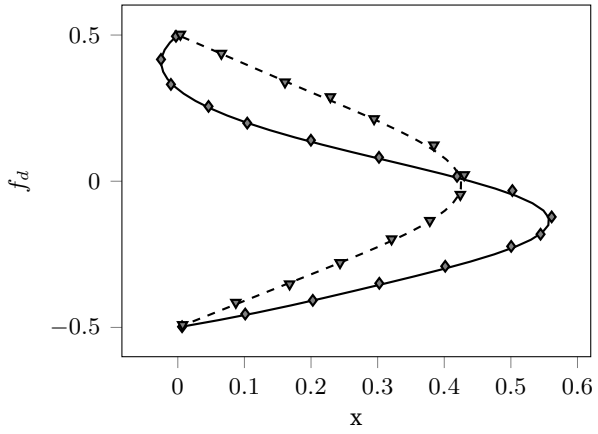

Figure 4.9: bla

4.2.2 Couette flow with vertical temperature gradient

As a first benchmark case to test the implemented low-Mach solver we analyse the Couette flow with a vertical temperature gradient. This configuration was already studied in (Klein et al., 2016), where the SIMPLE algorithm in a DG framework was used. We intend in this section to reproduce their results by using our fully coupled solver. We also show later how our implemented solver performs in relation to the SIMPLE based solver.

In Figure 4.10 a schematic representation of the testcase is shown. The top wall corresponds to a moving wall ($u = 1$) with a fixed temperature $T = T_h$. The bottom wall is a static one ($u = 0$), and has a constant temperature $T = T_c$. The domain is chosen as $\Omega = [0, 1] \times [0, 1]$, and Dirichlet boundary conditions are used for all boundaries. It is assumed that the fluid is composed of only one component, thus $N = 1$ and we can prescribe $Y_0 = 1.0$ everywhere in the domain. Additionally,the system is subjected to a gravitational field, where the gravity vector only has a component in the y direction. Under this conditions, the x-velocity, pressure and temperature are only dependent on the y coordinate, i.e. $u = u(y)$, $T = T(y)$ and $p = p(y)$.

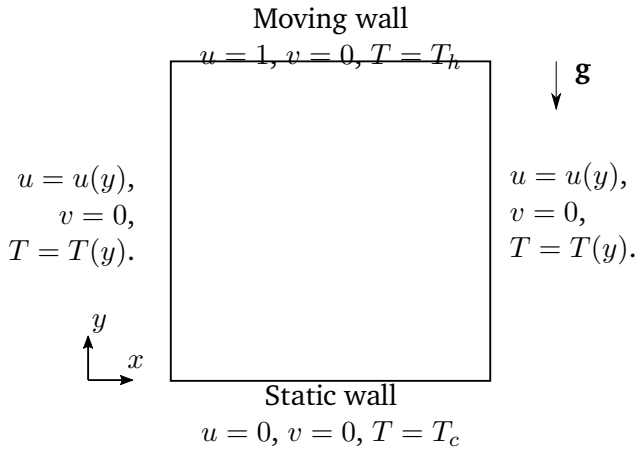

Figure 4.10: Schematic representation of the couette flow with temperature difference test case.

Thus, the governing equations (Equation (2.1)) reduce to

$$\frac{1}{\mathrm{Re}}\frac{\partial}{\partial y}\left(\mu\frac{\partial u}{\partial y}\right) = 0, \tag{4.5}$$

$$\frac{\partial p}{\partial y} = -\frac{\rho}{\mathrm{Fr}^2}, \tag{4.6}$$

$$\frac{1}{\mathrm{Re\,Pr}}\frac{\partial}{\partial y}\left(\lambda\frac{\partial T}{\partial y}\right) = 0. \tag{4.7}$$

It is possible to find an analytical solution for this problem. By assuming a temperature dependence of the transport properties according a Power Law ($\mu = \lambda = T^{2/3}$) a solution is obtained as

$$u(y) = C_1 + C_2\left(y + \frac{T_c^{5/3}}{T_h^{5/3} - T_c^{5/3}}\right)^{3/5}, \tag{4.8}$$

$$p(y) = -\frac{5p_0}{2\mathrm{Fr}^2}\frac{\left(y\left(T_h^{5/3} - T_c^{5/3}\right) + T_c^{5/3}\right)^{2/5}}{\left(T_h^{5/3} - T_c^{5/3}\right)} + C, \tag{4.9}$$

$$T(y) = \left(C_3 - \frac{5}{3}C_4 y\right)^{3/5}. \tag{4.10}$$

Where the constants C_1, C_2, C_3 and C_4 are determined by using the boundary conditions on

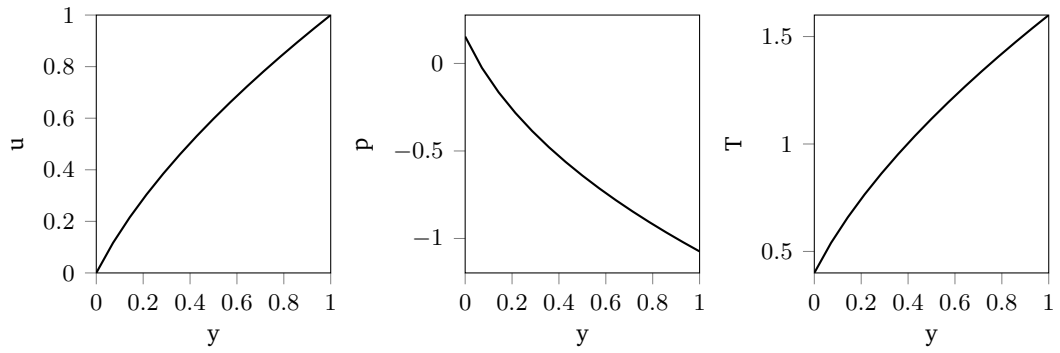

Figure 4.11: Solution of the Couette flow with vertical temperature gradient. Viscosity and heat conductivity are calculated with a Power-Law.

the top and bottom walls, and are given by

$$C_1 = \frac{\left(\frac{T_c^{5/3}}{T_h^{5/3}-T_c^{5/3}}\right)^{3/5}}{\left(\frac{T_c^{5/3}}{T_h^{5/3}-T_c^{5/3}}\right)^{3/5} - \left(\frac{T_h^{5/3}}{T_h^{5/3}-T_c^{5/3}}\right)^{3/5}} \tag{4.11}$$

$$C_2 = \frac{1}{\left(\frac{T_h^{5/3}}{T_h^{5/3}-T_c^{5/3}}\right)^{3/5} - \left(\frac{T_c^{5/3}}{T_h^{5/3}-T_c^{5/3}}\right)^{3/5}} \tag{4.12}$$

$$C_3 = T_c^{5/3}, \tag{4.13}$$

$$C_4 = \frac{3}{5}\left(T_c^{5/3} - T_h^{5/3}\right) \tag{4.14}$$

and again C is a real-valued arbitrary constant for the pressure.

For all calculations of this configuration shown in the following sections the dimensionless parameters are set as $\mathrm{Re} = 10$ and $\mathrm{Pr} = 0.71$, $T_h = 1.6$ and $T_c = 0.4$. Since we are dealing with an open system we set $p_0 = 1.0$. The Froude number is calculated as

$$\mathrm{Fr} = \left(\frac{2\mathrm{Pr}(T_h - T_c)}{(T_h + T_c)}\right)^{1/2} \tag{4.15}$$

In Figure 4.11 the solution for the velocity, pressure and temperature are shown. The results are for a mesh with 26×26 elements and a polynomial degree of three for u and T, and a polynomial degree of two for p.

h-convergence study

The convergence properties of the DG method for this non-isothermal system was studied using the analytical solution described before. The domain is discretized and solved in uniform Cartesian meshes with 16×16, 32×32, 64×64 and 128×128 elements. The polynomial degrees for the velocity and temperature are changed from 1 to 4 and for the pressure from 0

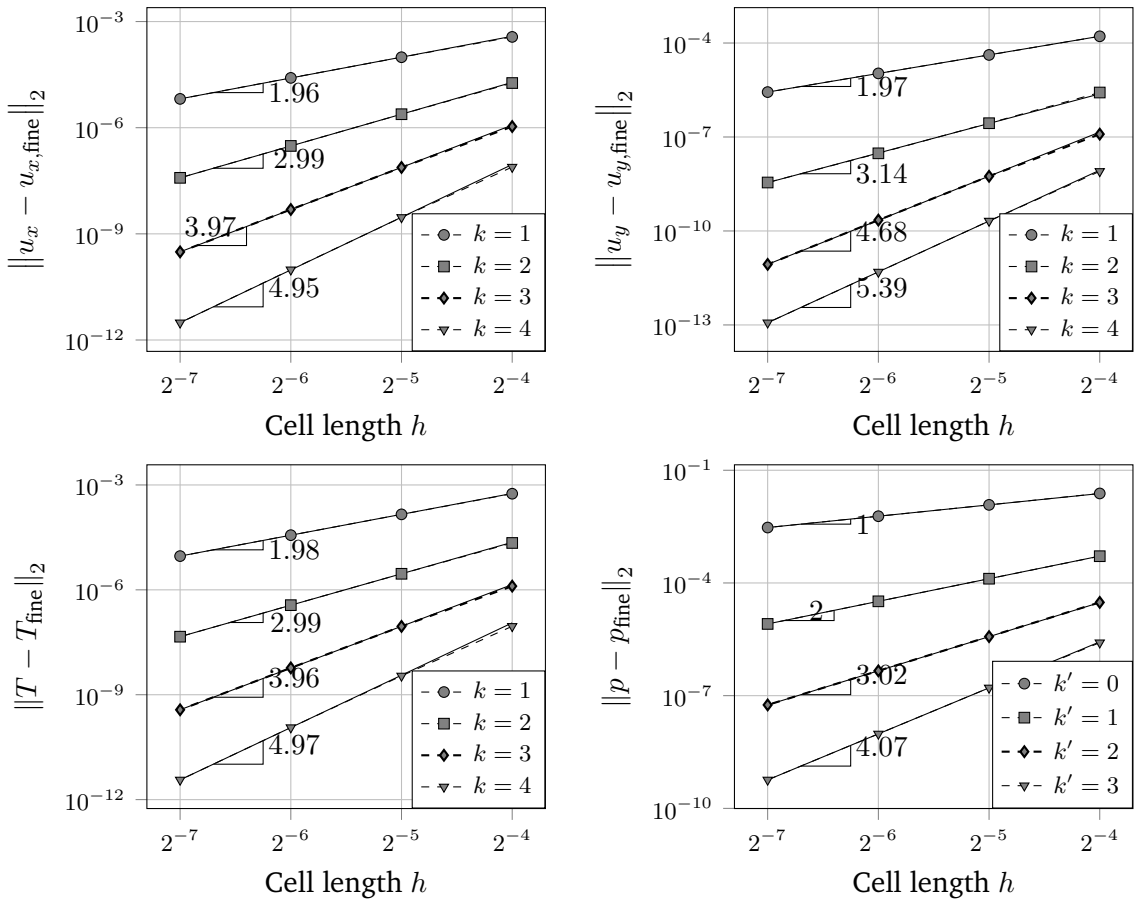

Figure 4.12: Convergence study of the differentially heated cavity problem for Ra $= 10^3$.

to 3. The convergence criteria described in Section 3.2.2 was used for all calculations. The analytical solution given by Equations (4.8) to (4.10) are as Dirichlet boundary conditions on all boundaries of the domain. The error is calculated against the analytical solution using the L^2 norm In Figure 4.12 the results of the h-convergence study are shown. We observe how the expected convergence rates are reached for all variables, namely a slope of the order $k + 1$ for both velocity components and the temperature, and a slope of $k' + 1$ for the pressure.

Comparison with SIMPLE

As mentioned before, a solver for solving low-Mach flows based on the SIMPLE algorithm (presented in Klein et al., 2016) has been already developed and implemented within the BoSSS framework. Though the solver was validated and shown to be useful for a wide variety of test cases, there were also disadvantages inherently associated with the SIMPLE algorithm. Within the solution algorithm, Picard-type iterations are used to search for a solution. This requires some prior knowledge from the user in order to select suitable relaxation factor values that provide stability to the algorithm, but at the same time do not slow down the computation substantially. It was also observed that the calculation times were prohibitively high for some test cases. This point motivated the development of the solver presented in the present work, where the system is solved in a monolytic way and and the Newton method globalized with a

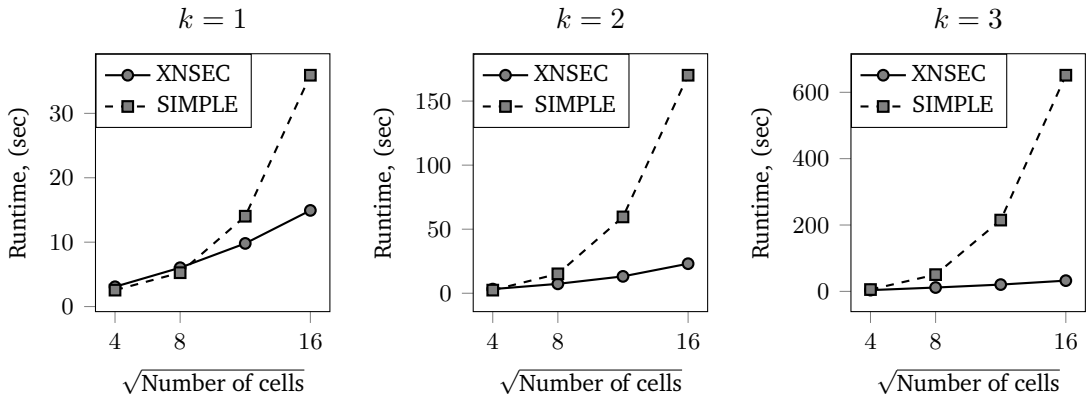

Table 4.2: Runtime comparison of the DG-SIMPLE algorithm (Klein et al., 2016) and the present solver (XNSEC) for the Couette flow with vertical temperature gradient configuration

Dogleg-type method is used to solve the system. We intend to show in this section a comparison of runtimes of the calculation of the Couette flow with vertical temperature gradient between the DG-SIMPLE algorithm (Klein et al., 2016) and the present solver (denoted here as XNSEC). Calculations were performed on uniform Cartesian meshes with 16×16, 32×32, 64×64 and 128×128 elements, and with varying polynomial degrees between 1 and 3 for the velocity and temperature, and between 0 y 2 for the pressure. All calculations where initialized with a zero velocity and pressure field, and with a temperature equal to one in the whole domain. Are calculations were performed single-core and the convergence criteria is set to 10^{-8} for both solvers. The under-relaxation factors for the SIMPLE algorithm were set for all calculations to 0.8, 0.5 and 1.0 for the velocity, pressure and temperature, respectively.

In figure Table 4.2 a comparison of the runtimes from both solvers is shown. It is clearly appreciated how the runtimes of the SIMPLE algorithm are higher for almost all of the cases studied. Obviously the under-relaxation parameters of the SIMPLE algorithm have an influence on the calculation times and an appropiate selection of them could decrease the runtimes. This is a clear disadvantage, because the selection of adequate factors is highly problem dependent and requires some previous expertise from the user. On the other hand, the globalized Newton method used by the XNSEC avoid this problem by using a more sophisticated method and heuristics in order to find a better path to the solution.

Bibliography

Armaly, B. F., Durst, F., Pereira, J. C. F., and Schönung, B. (1983). "Experimental and Theoretical Investigation of Backward-Facing Step Flow." In: *Journal of Fluid Mechanics* 127 (-1), p. 473. DOI: 10.1017/S0022112083002839.

Babuška, I. (1973). "The Finite Element Method with Lagrangian Multipliers." In: *Numerische Mathematik* 20.3, pp. 179–192. DOI: 10.1007/BF01436561.

Barkley, D., Gomes, G., and Henderson, R. (2000). "Three-Dimensional Instability in Flow over a Backward-Facing Step." In: *Journal of Fluid Mechanics* 473. DOI: 10.1017/S002211200200232X.

Bird, R. B., Stewart, W. E., and Lightfoot, E. N. (1960). *Transport Phenomena*. New York: Wiley. 780 pp.

Biswas, G., Breuer, M., and Durst, F. (2004). "Backward-Facing Step Flows for Various Expansion Ratios at Low and Moderate Reynolds Numbers." In: *Journal of Fluids Engineering* 126.3, pp. 362–374. DOI: 10.1115/1.1760532.

Botella, O. and Peyret, R. (1998). "Benchmark Spectral Results on the Lid-Driven Cavity Flow." In: *Computers & Fluids* 27, pp. 421–433. DOI: 10.1016/S0045-7930(98)00002-4.

Braack, M., Becker, R., Rannacher, R., and Warnatz, J. (1997). "An Adaptive Finite Element Method for Combustion Problems." In: *Proceedings of the Third Summer Conference, Numerical Modelling in Continuum Mechanics, Charles Universirt*.

Burke, S. P. and Schumann, T. E. W. (1928). "Diffusion Flames." In: *Industrial & Engineering Chemistry* 20.10, pp. 998–1004. DOI: 10.1021/ie50226a005.

Cockburn, B., Karniadakis, G. E., and Shu, C.-W. (2000). "The Development of Discontinuous Galerkin Methods." In: *Discontinuous Galerkin Methods*. Ed. by B. Cockburn, G. E. Karniadakis, and C.-W. Shu. Lecture Notes in Computational Science and Engineering. Berlin, Heidelberg: Springer, pp. 3–50. DOI: 10.1007/978-3-642-59721-3_1.

Dennis, J. E. and Schnabel, R. B. (1996). *Numerical Methods for Unconstrained Optimization and Nonlinear Equations*. Society for Industrial and Applied Mathematics. DOI: 10.1137/1.9781611971200.

Deuflhard, P. (2011). *Newton Methods for Nonlinear Problems*. Springer Series in Computational Mathematics. Berlin, Heidelberg: Springer Berlin Heidelberg. DOI: 10.1007/978-3-642-23899-4.

Dobbins, R. R. and Smooke, M. D. (2010). "A Fully Implicit, Compact Finite Difference Method for the Numerical Solution of Unsteady Laminar Flames." In: *Flow, Turbulence and Combustion* 85.3-4, pp. 763–799. DOI: 10.1007/s10494-010-9278-z.

Fernandez-tarrazo, E., Sanchez, A., Linan, A., and Williams, F. (2006). "A Simple One-Step Chemistry Model for Partially Premixed Hydrocarbon Combustion." In: *Combustion and Flame* 147.1-2, pp. 32–38. DOI: 10.1016/j.combustflame.2006.08.001.

Geisenhofer, M., Kummer, F., and Müller, B. (2019). “A Discontinuous Galerkin Immersed Boundary Solver for Compressible Flows: Adaptive Local Time Stepping for Artificial Viscosity–Based Shock-Capturing on Cut Cells.” In: *International Journal for Numerical Methods in Fluids* 91.9, pp. 448–472. DOI: 10.1002/fld.4761.

Girault, V., Rivière, B., and Wheeler, M. F. (2004). “A Discontinuous Galerkin Method with Nonoverlapping Domain Decomposition for the Stokes and Navier-Stokes Problems.” In: *Mathematics of Computation* 74.249, pp. 53–85. DOI: 10.1090/S0025-5718-04-01652-7.

Hennink, A., Tiberga, M., and Lathouwers, D. (2021). “A Pressure-Based Solver for Low-Mach Number Flow Using a Discontinuous Galerkin Method.” In: *Journal of Computational Physics* 425, p. 109877. DOI: 10.1016/j.jcp.2020.109877.

Hennink, A. (2022). “Low-Mach Number Flow and the Discontinuous Galerkin Method.” In: DOI: 10.4233/uuid:9b35b35a-0789-4883-a471-f8df0d7939ad.

Johnson, R. F. and Kercher, A. D. (2020). “A Conservative Discontinuous Galerkin Discretization for the Chemically Reacting Navier-Stokes Equations.” In: *Journal of Computational Physics* 423, p. 109826. DOI: 10.1016/j.jcp.2020.109826.

Karaa, S., Zhang, J., and Douglas, C. C. (2003). “Preconditioned Multigrid Simulation of an Axisymmetric Laminar Diffusion Flame.” In: *Mathematical and Computer Modelling* 38.3, pp. 269–279. DOI: 10.1016/S0895-7177(03)90086-0.

Kee, R. J., Coltrin, M. E., and Glarborg, P. (2003). *Chemically Reacting Flow: Theory and Practice*. Hoboken, N.J: Wiley-Interscience. 848 pp.

Keshtiban, I., Belblidia, F., and Webster, M. (2003). “Compressible Flow Solvers for Low Mach Number Flows—a Review.” In: 23.

Keyes, D. and Smooke, M. (1987). “Flame Sheet Starting Estimates for Counterflow Diffusion Flame Problems.” In: *Journal of Computational Physics* 73.2, pp. 267–288. DOI: 10.1016/0021-9991(87)90137-9.

Kikker, A., Kummer, F., and Oberlack, M. (2020). “A Fully Coupled High-Order Discontinuous Galerkin Solver for Viscoelastic Fluid Flow.” In: *International Journal for Numerical Methods in Fluids* (). DOI: 10.1002/fld.4950.

Klein, B., Kummer, F., and Oberlack, M. (2013). “A SIMPLE Based Discontinuous Galerkin Solver for Steady Incompressible Flows.” In: *Journal of Computational Physics* 237, pp. 235–250. DOI: 10.1016/j.jcp.2012.11.051.

Klein, B., Müller, B., Kummer, F., and Oberlack, M. (2016). “A High-Order Discontinuous Galerkin Solver for Low Mach Number Flows.” In: *International Journal for Numerical Methods in Fluids* 81.8, pp. 489–520. DOI: 10.1002/fld.4193.

Krause, D. and Kummer, F. (2017). “An Incompressible Immersed Boundary Solver for Moving Body Flows Using a Cut Cell Discontinuous Galerkin Method.” In: *Computers & Fluids* 153. DOI: 10.1016/j.compfluid.2017.05.008.

Kummer, F., Weber, J., and Smuda, M. (2021). “BoSSS: A Package for Multigrid Extended Discontinuous Galerkin Methods.” In: *Computers & Mathematics with Applications*. Development and Application of Open-source Software for Problems with Numerical PDEs 81, pp. 237–257. DOI: 10.1016/j.camwa.2020.05.001.

Kummer, F. (2012). “The BoSSS Discontinuous Galerkin Solver for Incompressible Fluid Dynamics and an Extension to Singular Equations.” PhD thesis. Darmstadt: Technische Universität.

Kummer, F. (2017). “Extended Discontinuous Galerkin Methods for Two-Phase Flows: The Spatial Discretization.” In: *International Journal for Numerical Methods in Engineering* 109.2, pp. 259–289. DOI: 10.1002/nme.5288.

Lv, Y. and Ihme, M. (2017). “High-Order Discontinuous Galerkin Method for Applications to Multicomponent and Chemically Reacting Flows.” In: *Acta Mechanica Sinica* 33, pp. 1–14. DOI: 10.1007/s10409-017-0664-9.

Majda, A. and Sethian, J. (1985). “The Derivation and Numerical Solution of the Equations for Zero Mach Number Combustion.” In: *Combustion Science and Technology* 42.3-4, pp. 185–205. DOI: 10.1080/00102208508960376.

Matalon, M., Ludford, G. S. S., and Buckmaster, J. (1980). “Diffusion Flames in a Chamber.” In: *Gasdynamics of Explosions and Reactive Systems*. Ed. by A. K. Oppenheim. Pergamon, pp. 943–959. DOI: 10.1016/B978-0-08-025442-5.50058-5.

Mcbride, B., Gordon, S., and Reno, M. (1993). *NASA Thermodynamic Data Base*. NASA Technical Memorandum 4513.

Müller, B. (1998). “Low-Mach-Number Asymptotics of the Navier-Stokes Equations.” In: *Journal of Engineering Mathematics* 34.1, pp. 97–109. DOI: 10.1023/A:1004349817404.

Nonaka, A., Day, M. S., and Bell, J. B. (2018). “A Conservative, Thermodynamically Consistent Numerical Approach for Low Mach Number Combustion. Part I: Single-level Integration.” In: *Combustion Theory and Modelling* 22.1, pp. 156–184. DOI: 10.1080/13647830.2017.1390610.

Pawlowski, R. P., Shadid, J. N., Simonis, J. P., and Walker, H. F. (2006). “Globalization Techniques for Newton–Krylov Methods and Applications to the Fully Coupled Solution of the Navier–Stokes Equations.” In: *SIAM Review* 48.4, pp. 700–721. DOI: 10.1137/S0036144504443511.

Pawlowski, R. P., Simonis, J. P., Walker, H. F., and Shadid, J. N. (2008). “Inexact Newton Dogleg Methods.” In: *SIAM Journal on Numerical Analysis* 46.4, pp. 2112–2132. JSTOR: 40233295.

Paxion, S., Baron, R., Gordner, A., Neuss, N., Bastian, P., Thévenin, D., and Wittum, G. (2001). “Development of a Parallel Unstructured Multigrid Solver for Laminar Flame Simulations with Detailed Chemistry and Transport.” In: *Numerical Flow Simulation II*. Ed. by E. H. Hirschel. Notes on Numerical Fluid Mechanics (NNFM). Berlin, Heidelberg: Springer, pp. 181–198. DOI: 10.1007/978-3-540-44567-8_11.

Peters, N. and Williams, F. A. (1987). “The Asymptotic Structure of Stoichiometric Methane-Air Flames.” In: *Combustion and Flame* 68.2, pp. 185–207. DOI: 10.1016/0010-2180(87)90057-5.

Peters, N. (1985). “Numerical and Asymptotic Analysis of Systematically Reduced Reaction Schemes for Hydrocarbon Flames.” In: *Numerical Simulation of Combustion Phenomena*. Ed. by R. Glowinski, B. Larrouturou, and R. Temam. Lecture Notes in Physics. Berlin, Heidelberg: Springer, pp. 90–109. DOI: 10.1007/BFb0008654.

Pietro, D. A. D. and Ern, A. (2012). *Mathematical Aspects of Discontinuous Galerkin Methods*. Mathématiques et Applications. Berlin Heidelberg: Springer-Verlag.

Poinsot, T. and Veynante, D. (2005). *Theoretical and Numerical Combustion*. R.T. Edwards, Inc. 544 pp. Google Books: cqFDkeVABYoC.

Rehm, R. and Baum, H. (1978). "The Equations of Motion for Thermally Driven, Buoyant Flows." In: *Journal of Research of the National Bureau of Standards* 83.3, p. 297. DOI: 10.6028/jres.083.019.

Rhebergen, S., Cockburn, B., and van der Vegt, J. J. (2013). "A Space–Time Discontinuous Galerkin Method for the Incompressible Navier–Stokes Equations." In: *Journal of Computational Physics* 233, pp. 339–358. DOI: 10.1016/j.jcp.2012.08.052.

Schenk, O., Gärtner, K., and Fichtner, W. (2000). "Efficient Sparse LU Factorization with Left-Right Looking Strategy on Shared Memory Multiprocessors." In: *BIT Numerical Mathematics* 40.1, pp. 158–176. DOI: 10.1023/A:1022326604210.

Schenk, O. and Gärtner, K. (2002). "Two-Level Dynamic Scheduling in PARDISO: Improved Scalability on Shared Memory Multiprocessing Systems." In: *Parallel Computing* 28.2, pp. 187–197. DOI: 10.1016/S0167-8191(01)00135-1.

Schenk, O. and Gärtner, K. (2004). "Solving Unsymmetric Sparse Systems of Linear Equations with PARDISO." In: *Future Generation Computer Systems*. Selected Numerical Algorithms 20.3, pp. 475–487. DOI: 10.1016/j.future.2003.07.011.

Shahbazi, K., Fischer, P. F., and Ethier, C. R. (2007). "A High-Order Discontinuous Galerkin Method for the Unsteady Incompressible Navier–Stokes Equations." In: *Journal of Computational Physics* 222.1, pp. 391–407. DOI: 10.1016/j.jcp.2006.07.029.

Shadid, J. N., Tuminaro, R. S., and Walker, H. F. (1997). "An Inexact Newton Method for Fully Coupled Solution of the Navier–Stokes Equations with Heat and Mass Transport." In: *Journal of Computational Physics* 137.1, pp. 155–185. DOI: 10.1006/jcph.1997.5798.

Shahbazi, K. (2005). "An Explicit Expression for the Penalty Parameter of the Interior Penalty Method." In: *Journal of Computational Physics* 205.2, pp. 401–407. DOI: 10.1016/j.jcp.2004.11.017.

Shen, W., Zhang, J., and Yang, F. (2006). "Newton's Method for Steady and Unsteady Reacting Flows." In: *ACM-SE 44*. DOI: 10.1145/1185448.1185621.

Smooke, M. D., Mitchell, R. E., and Keyes, D. E. (1986). "Numerical Solution of Two-Dimensional Axisymmetric Laminar Diffusion Flames." In: *Combustion Science and Technology* 67.4-6, pp. 85–122. DOI: 10.1080/00102208908924063.

Smoke, M. D. and Giovangigli, V. (1991). "Formulation of the Premixed and Nonpremixed Test Problems." In: *Reduced Kinetic Mechanisms and Asymptotic Approximations for Methane-Air Flames: A Topical Volume.* Ed. by M. D. Smooke. Lecture Notes in Physics. Berlin, Heidelberg: Springer, pp. 1–28. DOI: 10.1007/BFb0035363.

Smooke, M. D. and Giovangigli, V. (1992). "Numerical Modeling of Axisymmetric Laminar Diffusion Flames." In: *IMPACT of Computing in Science and Engineering* 4.1, pp. 46–79. DOI: 10.1016/0899-8248(92)90016-2.

Stauch, R., Lipp, S., and Maas, U. (2006). "Detailed Numerical Simulation of the Auto-Ignition of Liquid Fuel Droplets." In: *Advances in High Performance Computing and Computational Sciences.* Ed. by Y. Shokin, M. Resch, N. Shokina, N. Danaev, and M. Orunkhanov. Berlin, Heidelberg: Springer, pp. 127–137. DOI: 10.1007/978-3-540-33844-4_11.

Stauch, R. and Maas, U. (2007). “The Auto-Ignition of Single n-Heptane/Iso-Octane Droplets.” In: *International Journal of Heat and Mass Transfer* 50.15, pp. 3047–3053. DOI: 10.1016/j.ijheatmasstransfer.2006.12.005.

Sutherland, W. (1893). “LII. *The Viscosity of Gases and Molecular Force*.” In: *The London, Edinburgh, and Dublin Philosophical Magazine and Journal of Science* 36.223, pp. 507–531. DOI: 10.1080/14786449308620508.

Westbrook, C. K. and Dryer, F. L. (1981). “Simplified Reaction Mechanisms for the Oxidation of Hydrocarbon Fuels in Flames.” In: *Combustion Science and Technology* 27.1-2, pp. 31–43. DOI: 10.1080/00102208108946970.

Williams, F. A. (2000). *Combustion Theory: The Fundamental Theory of Chemically Reacting Flow Systems*. 2. ed., [Nachdr.] Combustion Science and Engineering Series. Cambridge, Mass: Perseus Books. 680 pp.

Xie, W. and Xi, G. (2016). “Fluid Flow and Heat Transfer Characteristics of Separation and Reattachment Flow over a Backward-Facing Step.” In: *International Journal of Refrigeration* 74. DOI: 10.1016/j.ijrefrig.2016.10.006.

Curriculum vitae

Vor- und Nachname

Persönliche Daten

Geburtsdatum:	-
Geburtsort:	-
Staatsangehörigkeit:	-

Schulbildung

Jahr - Jahr	-
Jahr - Jahr	-

Studium

Jahr - Jahr	-

Wissenschaftliche Tätigkeit

Jahr - Jahr	Wissenschaftlicher Mitarbeiter am Fachgebiet für Strömungsdynamik im Fachbereich Maschinenbau der TU Darmstadt, Promotion und Lehrtätigkeit